Platinum Group Thiophenoxyimine Complexes: Syntheses, Crystallographic and Computational Studies of Structural Properties

Jamin L. Krinsky, John Arnold, Robert G. Bergman**

Department of Chemistry, University of California, Berkeley, California, 94720

Abstract. Monomeric thiosalicylaldiminate complexes of rhodium(I) and iridium(I) were prepared by ligand transfer from the homoleptic zinc(II) species. In the presence of strongly donating ligands, the iridium complexes undergo insertion of the metal into the imine carbon-hydrogen bond. Thiophenoxyketimines were prepared by non-templated reaction of *o*-mercaptoacetophenone with anilines, and were complexed with rhodium(I), iridium(I), nickel(II) and platinum(II). X-ray crystallographic studies showed that while the thiosalicylaldiminate complexes display planar ligand conformations, those of the thiophenoxyketiminates are strongly distorted. Results of a computational study were consistent with a steric-strain interpretation of the difference in preferred ligand geometries.

Introduction

Transition metal complexes bearing salicylaldiminate ligands have been employed successfully in a wide variety of catalytic systems. Research regarding this ligand class has been greatly facilitated by their ease of synthesis: A large range of structures can be accessed, often requiring only one synthetic step from the many commercially available salicylaldehydes and amines (Equation 1). Jacobsen *et al.*

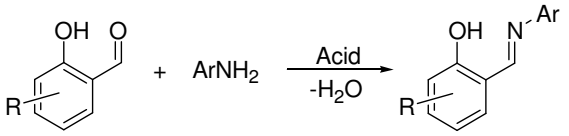

(1)

have developed a highly efficient olefin epoxidation system employing a tetradentate (salen-type) derivative (Figure 1a).[1] Titanium and zirconium complexes of bidentate salicylaldiminates have proven to be extremely active catalysts in the production of polyolefins.[2] Grubbs and others have further extended the utility of these ligands with respect to olefin polymerization, developing neutral, functional-group tolerant nickel catalysts (Figure 1b).[3] These late transition metal catalysts, however,

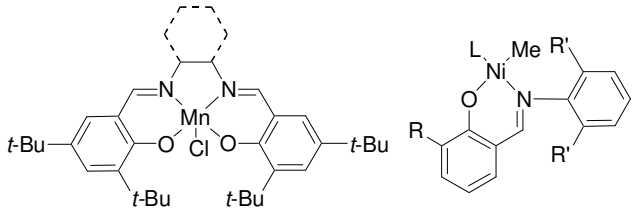

Figure 1a. Jacobsen epoxidation catalyst (salen-type ligand) **b.** Olefin polymerization catalyst (bidentate salicylaldiminate ligand).

tend to undergo deactivating ligand redistribution reactions unless very sterically demanding salicylaldiminates are used.[4] Examples of heavier platinum-group metal complexes are present in the literature[5] and some small-molecule reactivity has been explored.[6] However, ligand lability of the bidentate salicylaldiminates has limited their utility as supporting ligands.[7]

In place of the phenolate functionality of salicylaldiminates, thiosalicylaldiminates possess a thiophenolate moiety which might be expected to form a relatively inert bond with soft, polarizable metals. Homoleptic, first-row transition and main-group element complexes are known for iron through copper and the zinc triad, and incorporate bidentate, tridentate, and tetradentate ligand variants;[8] in addition, a few palladium species have been prepared.[9] While these complexes have been known for some time, their behavior as supporting ligands during metal-centered transformations is largely unexplored.[10] A major obstacle to their investigation has been the instability[11] of free thiosalicylaldimines: condensation of 2-mercaptobenzaldehyde with amines frequently results in the formation of dithiocin derivatives (Scheme 1a).[12] This limitation can be overcome using a templated

synthetic approach wherein a pre-formed metal-aldehyde complex is treated with the appropriate amine (Scheme 1b).[13] However, the approach is limited to cases where the metal-aldehyde complex precursor

Scheme 1.

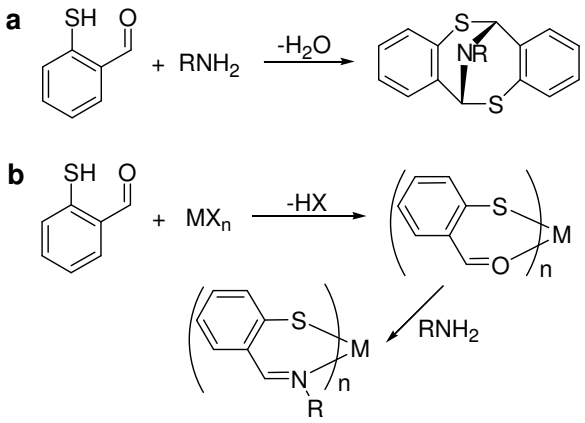

is stable, which we have found excludes the second and third-row platinum group metals in low oxidation states. Reported herein are rational synthetic routes to heteroleptic thiosalicylaldiminate and thiophenoxyketimine complexes of rhodium, iridium, nickel and platinum. Following that is a discussion of the structures and properties of these new species, including a surprising flexibility in ligand-coordination behavior.

Results and Discussion

Preparation and Structural Properties of Thiosalicylaldiminate Complexes. Early in our investigations it became evident that established synthetic routes are not amenable to the preparation of late transition metal thiosalicylaldiminate complexes. Treatment of dichlorobis(1,5-cyclooctadiene)diiridium with sodium 2-formylbenzenethiolate resulted in a product mixture that appeared by ^{1}H NMR to contain the desired iridium thiolate. However, this species decomposed over one hour at ambient temperature in solution, precluding its use as a synthon for further elaboration. Since the templated syntheses of the desired ligands were already proven effective when starting from the stable homoleptic zinc(II) aldehyde complexes,[14] it was postulated that reaction of thiosalicylaldiminate zinc species with platinum-group chlorides might provide an alternate synthetic route, much as dialkylzinc reagents alkylate platinum group chlorides (Scheme 2). Indeed, the

Scheme 2.

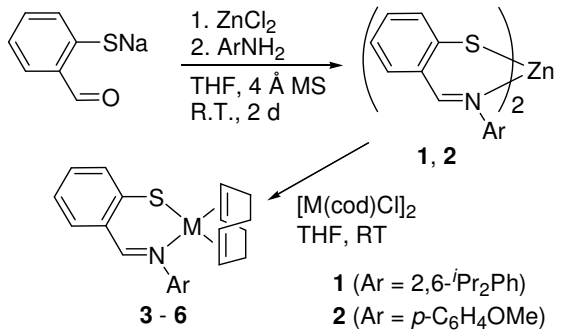

3 (M = Rh, Ar = 2,6-^{i}Pr$_2$Ph); **4** (M = Ir, Ar = 2,6-^{i}Pr$_2$Ph)
5 (M = Rh, Ar = *p*-C_6H_4OMe); **6** (M = Ir, Ar = *p*-C_6H_4OMe)

bis(thiosalicylaldiminate)zinc complexes cleanly exchange both ligands with rhodium(I) and iridium(I) chlorides, generating zinc chloride as an easily removable byproduct. Two ligands of differing steric demand were synthesized by the above templated route, one from 2,6-diisopropylaniline (prepared as $L^1{}_2Zn$ (**1**)) and one from *p*-anisidine (prepared as $L^2{}_2Zn$ (**2**)).[15] Both **1** and **2** undergo reaction with $[M(cod)Cl]_2$ to form $L^1M(cod)$ (M = Rh (**3**), Ir (**4**)) and $L^2M(cod)$ (M = Rh (**5**), Ir (**6**)[16]) in yields (isolated) ranging from 27% to 96%. All are stable, slightly air-sensitive solids which decompose in solution upon extended exposure to ambient atmosphere. The solids can be stored indefinitely under inert atmosphere and at ambient temperature. NMR spectra of each show only a single species present in solution that displays C_s symmetry. The solid-state structures of **4**, **5** and **6** were determined by X-ray diffraction analysis and are shown in Figures 2-4.[17]

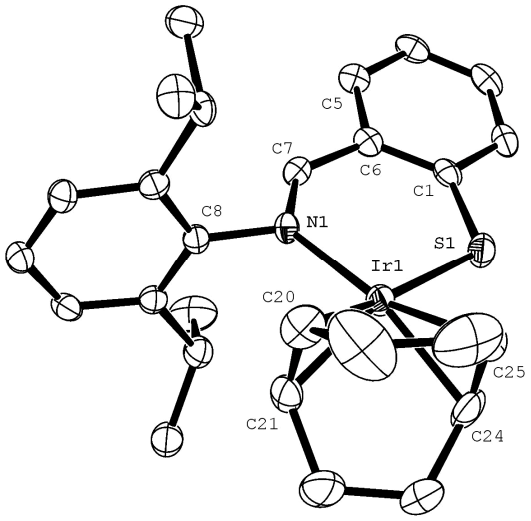

Figure 2. ORTEP diagram of **4** at 50% probability (H atoms omitted for clarity). Selected bond lengths (Å) and angles (°): Ir1-S1, 2.275(1); Ir1-N1, 2.081(3); Ir1-C20, 2.141(4); Ir1-C21, 2.149(4); Ir1-C24, 2.148(4); Ir1-C25, 2.138(5); S1-C1, 1.730(4); N1-C7, 1.304(5); C6-C7, 1.436(5); S1-Ir1-N1, 92.74(8); N1-C7-C6-C5, 173.7(4).

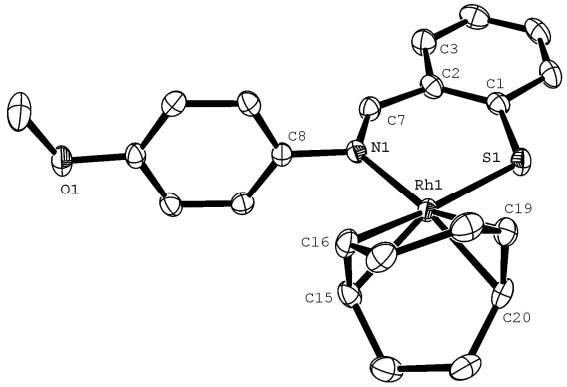

Figure 3. ORTEP diagram of **5** at 50% probability (H atoms omitted for clarity). Selected bond lengths (Å) and angles (°): Rh1-S1, 2.2755(6); Rh-N1, 2.098(2); Rh1-C15, 2.160(2); Rh1-C16, 2.175; Rh1-C19, 2.147(2); Rh1-C20, 2.165(2); S1-C1, 1.727(2); N1-C7, 1.311(3); C2-C7, 1.436(3); S1-Rh1-N1, 92.68(5); N1-C7-C2-C3, 178.8(2).

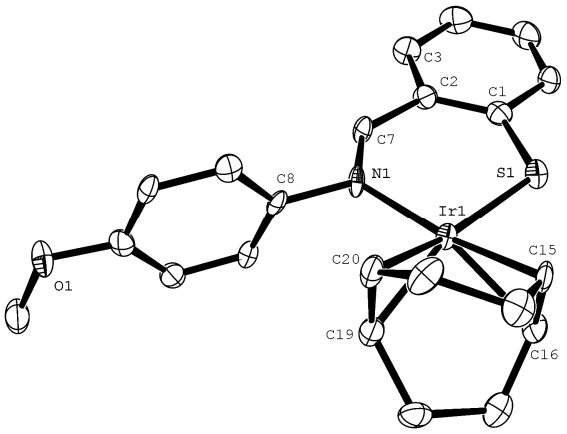

Figure 4. ORTEP diagram of **6** at 50% probability (H atoms omitted for clarity). Selected bond lengths (Å) and angles (°): Ir1-S1, 2.268(2); Ir1-N1, 2.077(7); Ir1-C15, 2.146(9); Ir1-C16, 2.133(9); Ir1-C19, 2.141(9); Ir1-C20, 2.162(9); S1-C1, 1.734(9); N1-C7, 1.32(1); C2-C7, 1.45(1); S1-Ir1-N1, 93.5(2); N1-C7-C2-C3, 177.8(10).

The monomeric nature of complexes **4**, **5** and **6** is somewhat surprising, given the tendency of sterically unencumbered aryl sulfides to bridge two metal centers through the sulfur atom.[18] This structural feature is particularly noteworthy given the absence of any sterically demanding substituents on L^2. The ligand backbone in each structure is essentially planar, with the metal lying close to this approximate plane. In the case of **6**, the greatest deviation from the least-squares plane defined by the iridium center and the atoms making up the chelate ring is 0.033(9) Å. Compound **4** displays a slight bending of the iridium center out of the plane defined by the chelate ring, a distortion common among complexes containing π-conjugated chelating ligands such as β-diketiminates.[19] The thiophenoxy-imine

C-C bond lengths of **4**, **5** and **6** are 1.436(5), 1.436(3) and 1.448(10) Å, respectively. These bond lengths are contracted relative to those of a carbon-carbon single bond and thus are consistent with the conclusion that L^1 and L^2 behave as rigid, π-conjugated ligands.

Reaction of iridium complexes with trimethylphosphine. Attempts to exchange the coordinated cod ligands on **4** or **6** with trimethylphosphine did not yield the expected bis-phosphine complexes. Treatment of **4** or **6** with excess trimethylphosphine at room temperature resulted in the immediate formation of yellow solutions having ^{1}H NMR spectra consistent the coordination of two geometrically equivalent phosphine ligands. Surprisingly, no free cod is observed. Instead, resonances exist that correspond to symmetrically bound cod (Equation 2). These cod resonances are quite broad, suggesting

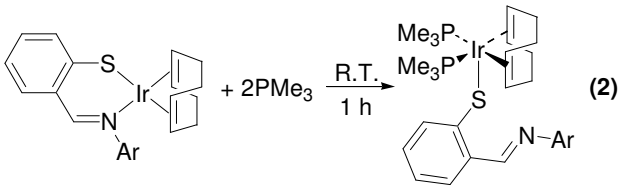

4, 6 **7, 8** **(2)**

fluxional behavior at ambient temperature. The products arising from **4** and **6** were therefore assigned the formulae $L^1Ir(cod)(PMe_3)_2$ (**7**) and $L^2Ir(cod)(PMe_3)_2$ (**8**), respectively. Proton-decoupled ^{31}P NMR spectra show only a single phosphine resonance for each species. The structural motif that is most consistent with these data is a square pyramidal geometry with two phosphine ligands and cod occupying the basal positions and the thiolate sulfur occupying the apical position. Thus the thiosalicylaldiminate ligand is probably bound in a monodentate fashion.

Phosphine complex **8** decomposed to a complex mixture of unidentified compounds over a period of about one day in benzene solution or upon attempted isolation. While **7** was equally unstable, its decomposition products were regenerated **4** and the new phosphine-containing compound **9**. Heating a mixture of **4** and **9** for 30 minutes in the presence of added trimethylphosphine resulted in the clean conversion of the remaining **4** to **9**. Heating a mixture of **4** and three equivalents of the phosphine also cleanly generated **9**. Compound **9** exhibits an ^{1}H NMR signal consisting of an apparent doublet of triplets centered at -10.75 ppm (J = 156 Hz, 18.2 Hz) that we attributed to a metal hydride species. The

absence of a signal for an imine proton suggested that site as the source of the hydride. Proton and proton-decoupled ^{31}P NMR spectra are consistent with the presence of three non-equivalent phosphine ligands. These data support the assignment of **9** as the iridium(III) species (L^1-H)Ir(PMe_3)$_3$H where L^1-H is the product of oxidative addition of the imine C-H bond of L^1 to the iridium(I) center of intermediate **7** (Equation 3). It is likely that **8** also undergoes this transformation, but the presumed iridium(III) product apparently reacts further to generate the complex mixture observed.

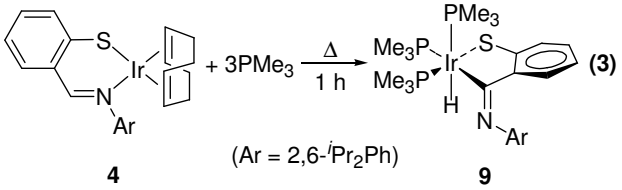

Structural elucidation of **9** by X-ray diffraction analysis confirmed the assignment made on the basis of spectroscopic data. The structure depicted in Figure 5 possesses a distorted octahedral geometry, with the atoms of the first coordination sphere bent towards the site occupied by the hydride ligand (not located). The P1-Ir1-P2 and P1-Ir1-P3 bond angles of 96.69(5) and 100.35(5)°, respectively, illustrate this distortion. The L^1-H chelate backbone is approximately coplanar with the plane defined by Ir1, S1 and C7. The orientation of the N-aryl ring explains the presence of two sets of isopropyl resonances in the ^1H NMR spectra of **9**. One isopropyl group is oriented near the phosphine ligand containing P1, rendering its two methyl groups diastereotopic. The other is situated in the hemisphere containing the sterically non-demanding hydride ligand and thus it can rotate, resulting in spectroscopically-equivalent methyl substituents. Rotation around the N-Ar bond is apparently slow on the NMR timescale.

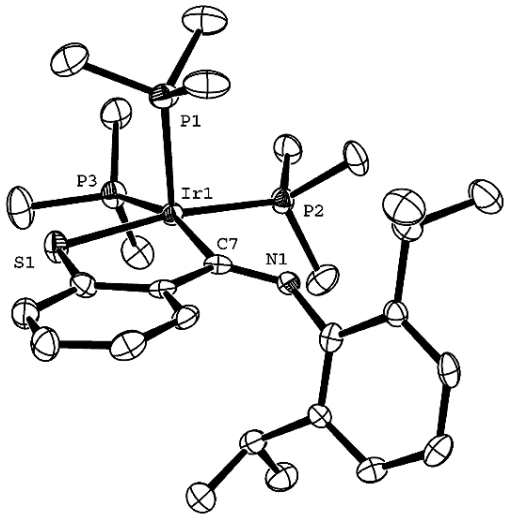

Figure 5. ORTEP diagram of **9** at 50% probability (H atoms omitted for clarity). Hydride not located. Selected bond lengths (Å) and angles (°): Ir1-S1, 2.380(1); Ir1-P1, 2.351(2); Ir1-P2, 2.288(1); Ir1-P3, 2.337(2); Ir1-C7, 2.097(5); S1-C1, 1.736(5); S1-Ir1-P1, 90.07(5); S1-Ir1-P2, 171.68(5); S1-Ir1-P3, 87.84(5); S1-Ir1-C7, 84.2(1); P1-Ir1-P2, 96.69(5); P1-Ir1-P3, 100.35(5); P1-Ir1-C7, 94.1(1).

Preparation of Thiophenoxyketimines. The observed proclivity towards imine C-H bond insertion of the thiosalicylaldiminates prompted us to explore derivatives of this ligand architecture which might be less prone to unwanted reactivity with the metal center. The most obvious derivatization is replacement of the aldimine hydrogen with a methyl group, affording the simplest ketimine (Scheme 3). To our knowledge only a few previous examples of this ligand class exist, all being of the tetradentate

Scheme 3.

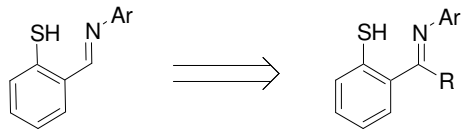

Thiophenoxy-aldimine

Thiophenoxy-ketimine

type prepared by templated routes discussed previously.[20] We found that the ketimines derived from sterically unhindered anilines can be prepared directly and in good yield if the reaction mixtures are kept at ambient temperature. Compounds L^3H (**10**, Ar = *p*-C_6H_4Me) and L^4H (**11**, Ar = *p*-C_6H_4OMe) are bright red, crystalline solids that are stable in the solid state and in solution provided they are stored under inert atmosphere. Like the free thiosalicylaldimines that have been successfully isolated,[12] they

display extremely downfield-shifted thiol resonances in their ^{1}H NMR spectra (17.3 and 18.2 ppm respectively) which are substantially outside of the typical diamagnetic region.

X-ray diffraction studies on a sample of **10** revealed that the thiol proton is in fact associated with the imine nitrogen, and the structure is better classified as intermediate between a thiolate zwitterion and a thioketone (Figure 6). This configuration had previously been proposed for the free thiosalicylaldimines based on spectroscopic data.[21] Iminium hydrogen H1 was located and its positional coordinates refined, while the other hydrogen atoms were placed in calculated positions. The C1-C2, C5-C6 and C1-C6 bond lengths are 1.418(3), 1.407(3) and 1.444(3) Å, respectively. These bond lengths are considerably greater

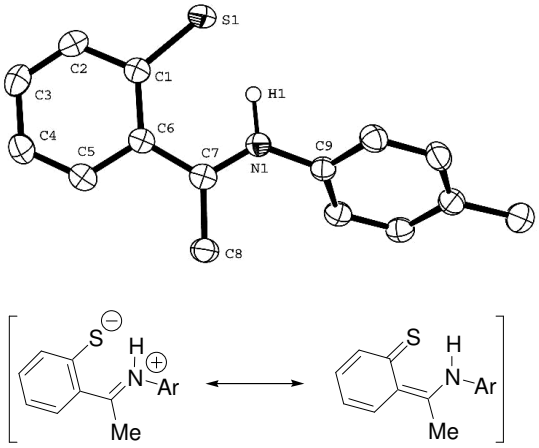

Figure 6. ORTEP diagram of **10** at 50% probability level. Calculated H atoms omitted for clarity. Selected bond lengths (Å) and angles (°): S1-C1, 1.739(2); N1-H1, 1.04(3); N1-C7, 1.308(3); C1-C2, 1.418(3); C2-C3, 1.360(3); C3-C4, 1.398(3); C4-C5, 1.371(3); C5-C6, 1.407(3); C1-C6, 1.444(3); C6-C7, 1.456(3); S1-C1-C2, 117.0(2); S1-C1-C6, 126.5(2); C5-C6-C7-C8, 0.2(3); C7-N1-C9-C14, 49.5(3).

than those of a completely delocalized phenyl ring, which in this structure average 1.388 Å for the N1-bound aryl ring. The C2-C3 and C4-C5 bond lengths are significantly contracted (1.360(3) and 1.371(3) Å respectively) and the C1-S1 bond length of 1.739(2) Å is somewhat short, lending support for contribution of the thioketone resonance form. The iminium-thiolate backbone is essentially planar, with a greatest deviation of 0.012(2) Å (C7) from the least squares plane defined by S1, C1, C6, C7 and N1. The N1-bound aryl group is rotated by 49.5(3)° with respect to this plane and thus is out of conjugation with the rest of the π-electron system.

Synthesis of Thiophenoxyketimine Complexes. The alkali metal salts of L^3 (generated in situ from **10**) reacted with a variety of metal halides to form the corresponding thiophenoxyketimine complexes.

Complexes of formulae $L^3M(cod)$ (M = Rh (**12**), Ir (**13**)) and $L^3M(PPh_3)_nX$ (M = Ni, X = Br, n = 1 (**14**); M = Pt, X = Cl, n = 1 (**15**), 2 (**16**)) were prepared from $[M(cod)Cl]_2$ and $(Ph_3P)_2MX_2$, respectively. The iridium system yielded multiple products when the reaction was scaled past 50 mg of **10**. However, when $Ir(cod)_2Cl$ was used in place of $[Ir(cod)Cl]_2$ the reaction proceeded to high yield (by NMR) on a 200 mg scale although separation of $L^3Ir(cod)$ (**13**) from the small percentage of byproducts drastically reduced the isolated yield. The known compound $Ir(cod)_2Cl$ exists as a mixture of $[Ir(cod)Cl]_2$ and free cod in THF solution, hence the increase in selectivity must be due in some way to the presence of the additional free cod. Stabilization of a reactive intermediate during the ligand substitution process is a possible explanation for this observation.

In the case where M = Ni, one phosphine ligand was cleanly displaced by L^3 to produce $L^3Ni(PPh_3)Br$ (**14**) quantitatively. However, incomplete phosphine displacement was observed with the platinum analog, resulting in an equilibrium mixture of $L^3Pt(PPh_3)Cl$ (**15**) and $L^3Pt(PPh_3)_2Cl$ (**16**). In the case of **16**, L^3 is presumably bound only through the thiophenylate sulfur. The proposed structure is analogous to that bearing a similar ligand which was crystallographically determined (see below). Reasonably pure **16** was isolated by concentrating a THF solution of the crude mixture in the presence of excess triphenylphosphine (analytically pure samples could not be obtained; NMR spectra are available as Supporting Information) (Scheme 4). While heating re-solvated **16** generated only a small amount of **15**, slow crystallization from the crude mixture (by pentane vapor diffusion) yielded crystalline **15** only. This observation suggests that crystal packing forces are sufficient to offset the energy increase in forming **15**. Surprisingly, pure **15** was also prepared by repeatedly washing solid **16** with Et_2O. The use of platinum starting materials containing more easily displaced ligands resulted only in intractable mixtures: no desired product was observed when $(PhCN)_2PtCl_2$ or $(Me_2S)_2PtCl_2$ were treated with L^3Na.

Scheme 4.

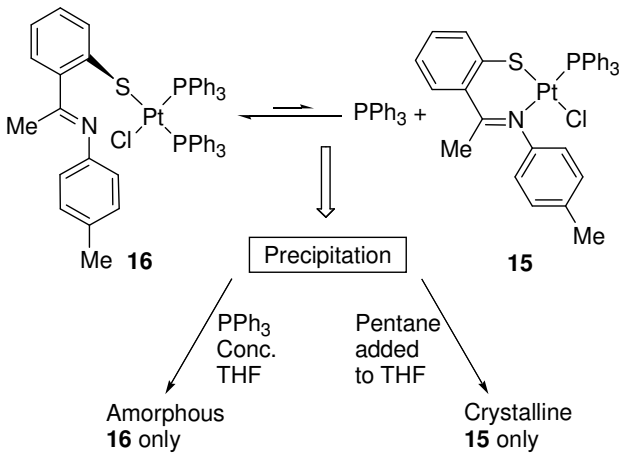

When L^4 was employed in place of L^3, a mixture of mono- and bis-phosphine complexes was again isolated. However, when $(Ph_3P)_2PtCl_2$ was treated with L^4Na at -78 °C under extremely dilute conditions (2.5 mM), $L^4Pt(PPh_3)Cl$ (**17**) and triphenylphosphine were the principal observed products. This observation implies that **17** is the kinetically-favored product of this reaction, while $L^4Pt(PPh_3)_2Cl$ (**18**) and **17** are of comparable thermodynamic stability. This is puzzling if one assumes the reaction proceeds via salt metathesis followed by displacement of the phosphine by the imine functionality of L^4. A satisfactory explanation for this reactivity has not been reached, as the heterogeneous nature of the reaction mixture has so far precluded kinetic study. Interestingly, the most effective method for isolation of pure **17** was the simple addition of diethyl ether over an amorphous sample of the crude product. Over the course of several hours all amorphous material was converted to crystalline product, leaving in solution the triphenylphosphine liberated during the reaction. The lattice energy gained apparently drives the transformation from amorphism to crystallinity through the small equilibrium concentration of dissolved product.

Compounds **12**-**15** and **17** are stable, crystalline materials that were unchanged after exposure to air for weeks in the solid state. In solution, no decomposition was observed over several months in the absence of oxygen. No ligand disproportionation was observed when nickel complex **14** was heated at 75 °C in benzene for 24 hours; thus it appears that thiophenoxyketimines do afford substitutionally inert ligands. With this in mind we wished to prepare hydrocarbyl nickel complexes that might be reactive towards olefins. However, treatment of $(Ph_3P)_2NiPhCl$ with alkali metal salts of L^3 resulted only in

intractable tars. There is evidence in the literature that aryl substituents on group 10 metals can reductively couple with aryl sulfides.[22] The coupling product was not observed in the product mixture, although this decomposition pathway cannot be ruled out as this particular diaryl sulfide might react further with the highly reactive zero-valent nickel species generated by the coupling reaction.

In order to verify that classical organometallic complexes bearing thiophenoxyketimine ligands can exist, alkyl substituents were then investigated. Attempted alkylations of **14** with MeLi, MeMgBr or Me_2Zn all resulted in decomposition to intractable material. This route seems to be generally avoided with respect to the salicylaldiminate complexes, suggesting a lack of compatibility with the ligand's imine fragment. Due to the comparatively facile synthesis of alkylplatinum starting materials, these were chosen for subsequent study. The reaction of $(Ph_3P)_2PtMeCl$ with L^3Na yielded multiple uncharacterized species. While heating $(Ph_3P)_2PtMe_2$ in the presence of **10** or **11** resulted only in the decomposition of the ligand, $(nbd)PtMe_2$ (nbd = norbornadiene) reacted with **11** at ambient temperature in acetonitrile (Equation 4), spontaneously precipitating a modest yield of an impure material formulated as L^4PtMe_3 (**19**) on the basis of ^1H NMR spectra (available as Supporting Information). Purification of this material has proven problematic and thus the complex is not fully characterized.

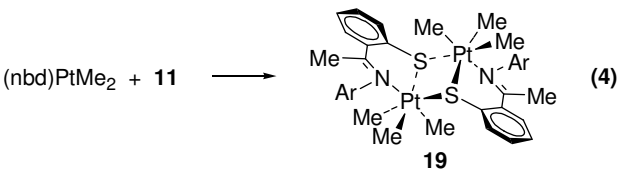

A few high-quality crystals of **19** formed when the reaction mixture was allowed to stand, and this material was subjected to X-ray crystallographic analysis. Complex **19** is a centrosymmetric dimer wherein each sulfur atom bridges both platinum centers and each imine nitrogen binds to one of the two platinum centers (Figure 7). Interestingly, **19** is a structural analog of the known salicylaldiminate complex formulated as $[(salnr)PtMe_3]_2$.[23] The geometry about the platinum(IV) center is only slightly

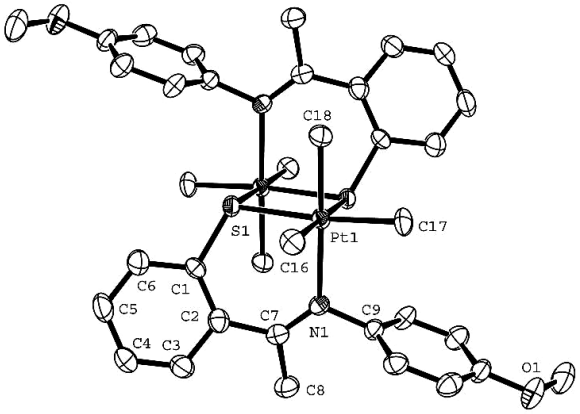

Figure 7. ORTEP diagram of **19** at 50% probability level. H atoms omitted for clarity. Selected bond lengths (Å) and angles (°): Pt1-S1, 2.391(1); Pt1-N1, 2.198(4); Pt1-C16, 2.060(5); Pt1-C17, 2.071(5); Pt1-C18, 2.052; S1-C1, 1.754(5); C2-C7, 1.490(7); S1-Pt1-N1, 89.6(1); S1-Pt1-C16, 95.1(2); S1-Pt1-C17, 174.5(2); S1-Pt1-C18, 89.4(2); N1-Pt1-C18, 178.4(2); C3-C2-C7-C8, 32.5(7).

distorted from the idealized octahedron. The Pt-Pt separation is 3.68 Å. Unlike the thiosalicylaldiminate complexes described above, the chelating ligand backbone is non-planar with a twist about the C2-C7 bond of 32.5(7)°. The C2-C7 bond length is 1.490(7) Å which is significantly longer than the analogous bond length of 1.456(3) Å in the free ligand **10**. Thus the imine moiety and the thiophenylate ring are extensively deconjugated. The platinum-bound methyl group containing C17 is situated over the nitrogen-bound aryl ring. The close proximity of these two substituents apparently prevents rotation about the N1-C9 bond, which explains the observation that all of the aryl proton resonances (for each asymmetric unit) in the ^{1}H NMR spectrum of **19** are non-equivalent.

Reactivity of a triarylphosphine with thiophenoxyketimine complexes 12, 13. Rhodium complex **12** reacted cleanly with two equivalents P(*p*-tol)$_3$ to form L^{3}Rh(P(*p*-tol)$_3$)$_2$ (**20**) over 8 h (Scheme 5). Monitoring the reaction by ^{1}H NMR (C_6D_6) revealed that no **12** was left in solution after 1 h. In addition to **20** and free cod, a third species was present in solution that gave rise to olefinic cod resonances at 5.09 and 3.45 ppm, one of which was significantly shifted relative to that of **12** (4.64 and 3.45 ppm). Proton-decoupled ^{31}P NMR spectra of the mixture show resonances corresponding to **20**, free P(*p*-tol)$_3$ and a doublet ($J_{P\text{-}Rh}$ = 153.9 Hz) consistent with a mono-phosphine rhodium complex. These data are consistent with an intermediate wherein one phosphine is bound to rhodium with retention of the cod ligand. The downfield cod resonance is significantly upfield-shifted relative to free cod (5.58 ppm),

indicating that both olefinic moieties are still bound to rhodium. Thus the intermediate is assigned as $L^3Rh(cod)P(p\text{-tol})_3$ (**21**) where L^3 is bound only through the thiolate sulfur.

Scheme 5.

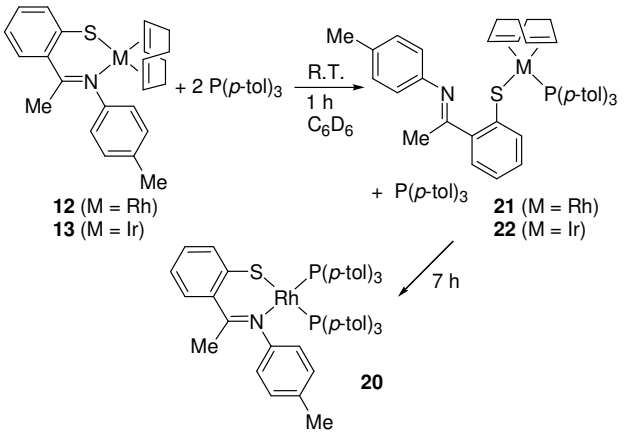

Complex **22**, the iridium analog of **21**, was observed after 1 h in C_6D_6 and was the only species present in solution (other than 1 equiv of free $P(p\text{-tol})_3$). Olefinic resonances in the ^1H NMR spectra occur at 5.07 and 3.89 ppm (compared with 4.54 and 3.05 ppm for **13**). Phosphorous NMR spectra display only two resonances in a one-to-one ratio, one corresponding to free $P(p\text{-tol})_3$ and the other occurring at 22.10 ppm. No final product analogous to **20** was observed after allowing the reaction to proceed for 48 h. While this species appeared stable in solution at ambient temperature, heating or attempted isolation yielded intractable material.

The hemilabile nature of L^3 indicates that this ligand behaves more like a thiophenylate ligand with a tethered imine fragment than a rigid, conjugated ligand such as a β-diketiminate. The instability of the ligand towards alkylating agents supports this conclusion, as the alkylation of β-diketiminate-bearing complexes is a well-known transformation.[24] Therefore we wished to investigate structural aspects of these complexes that may impart the observed reactivity.

Crystallographic/Computational Analysis of Ligand Conformation. Several species bearing chelating L^3 or L^4 were subjected to X-ray crystallographic analysis, confirming the structural assignments made by spectroscopic means. All are square planar complexes with unremarkable bond lengths and angles around the metal centers. The nickel-containing species **14** is slightly distorted

towards a tetrahedral conformation. Representative structures are depicted in Figures 8-10 (see Schemes 4 and 5 for line drawings).

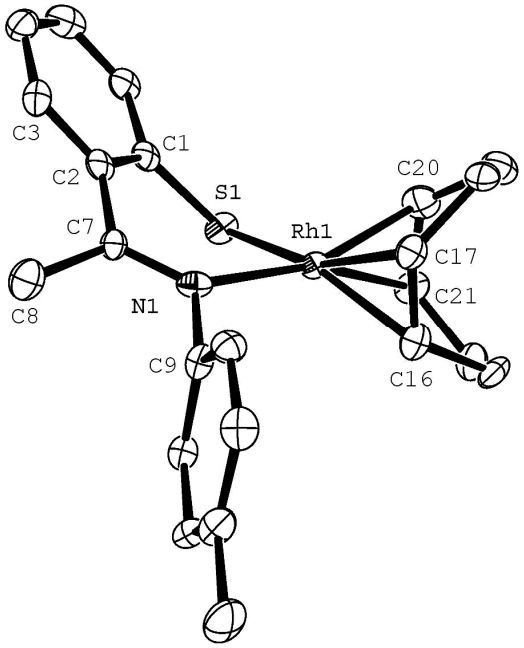

Figure 8. ORTEP diagram of **12** at 50% probability. One of two molecules in the asymmetric unit displayed. H atoms omitted for clarity. Selected bond lengths (Å) and angles (°): Rh1-S1, 2.314(2); Rh1-N1, 2.145(5); Rh1-C16, 2.183(7); Rh1-C17, 2.163(6); Rh1-C20, 2.125(7); Rh1-C21, 2.128(6); S1-C1, 1.744(6); N1-C7, 1.307(8); C2-C7, 1.477(9); S1-Rh1-N1, 88.2(1); C3-C2-C7-C8, 35.0(7).

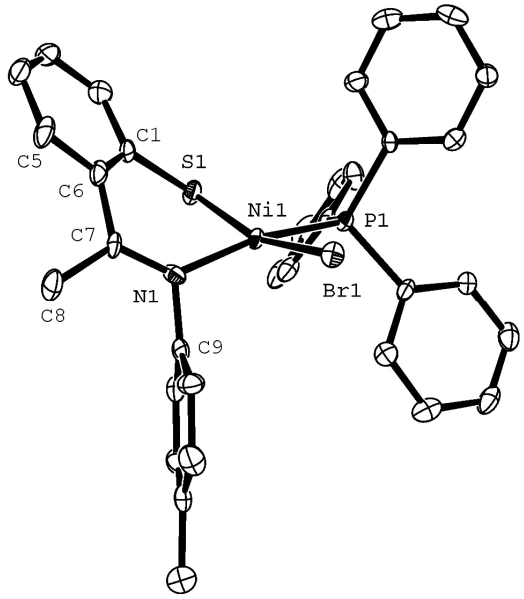

Figure 9. ORTEP diagram of **14** at 50% probability. H atoms omitted for clarity. Selected bond lengths (Å) and angles (°): Br1-Ni1, 2.362(1); Ni1-S1, 2.149(2); Ni1-P1, 2.184(2); Ni1-N1, 1.911(5); S1-C1,

1.759(7); N1-C7, 1.284(8); C6-C7, 1.473(9); Br1-Ni1-P1, 89.50(6); Br1-Ni1-N1, 93.8(2); S1-Ni1-P1, 90.77(7); S1-Ni1-N1, 89.9(2); C5-C6-C7-C8, 27.3(9).

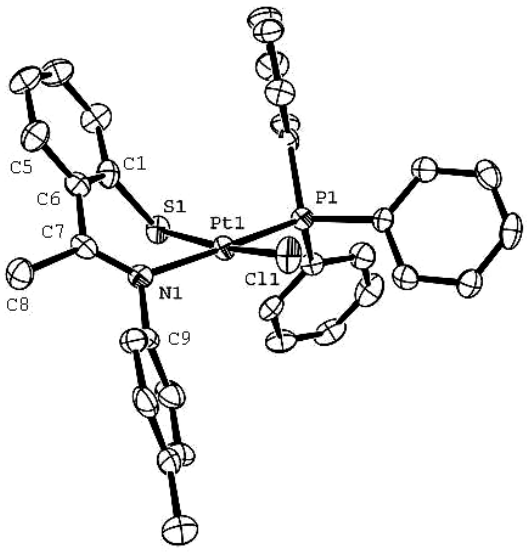

Figure 10. ORTEP diagram of **15** at 50% probability. H atoms omitted for clarity. Selected bond lengths (Å) and angles (°): Pt1-Cl1, 2.333(2); Pt1-S1, 2.283(2); Pt1-P1, 2.220(2); Pt1-N1, 2.101(5); S1-C1, 1.779(7); N1-C7, 1.293(8); C6-C7, 1.473(9); Cl1-Pt1-P1, 95.42(6); Cl1-Pt1-N1, 89.4(1); S1-Pt1-P1, 88.25(6); S1-Pt1-N1, 87.0(1); C5-C6-C7-C8, 37.3(9).

The most striking feature revealed by X-ray crystallographic investigation is the lack of ligand planarity observed for the ketimine complexes. Whereas the solid-state structures of the aldimine complexes **4**, **5** and **6** display approximate C_s symmetry with the metal and chelating ligand backbone defining the mirror plane, the ketimine analogs possess an extremely non-planar ligand conformation. The thiolate phenyl ring is sharply canted with respect to the plane containing the metal and atoms of the first coordination sphere. The carbon-carbon bond connecting the thiophenylate moiety with the imine fragment is twisted such that π-electron conjugation of the imine and thiophenylate π-electron systems is lost. This geometry is observed in the solid-state structures of some nickel thiosalicylaldiminate complexes; however, there appears to be no trend in substitution pattern that would explain why some are planar and some bent.[8b,25] Thus it appears that in those reported systems the lack of planarity is due primarily to crystallographic packing forces.

We wished to investigate by computational methods whether the marked difference in ligand conformation between the aldimines and ketimines is due to steric factors or an unexpected electronic effect. This problem is well suited to DFT computations because only geometries (not relative energies)

were compared, which are usually quite accurately modeled using this method.[26] All calculations were performed at the B3LYP/LACVP** level of theory, unless otherwise noted. As a starting point, the structures of the aldimine and ketimine complexes that were determined crystallographically were optimized and were found to agree well with the experimentally observed structures.

In order to check for the presence of a planar structure as a local energy minimum in the case of the methyl ketimine complexes, the geometry of **12** was first optimized with the ligand backbone and metal-chelate ring constrained in a planar conformation. The constraints were then removed, and the optimization was performed once again. A bent structure identical to that previously calculated was obtained, indicating that there is no energy minimum at the planar geometry. The bent geometry was found to be 4.6 kcal/mol (not ZPE-corrected) lower in energy than the planar geometry. When the optimized structure of **12** was modified such that the imine methyl group was replaced by a hydrogen atom, re-optimization of that structure yielded a planar geometry. Thus, the aldimine and ketimine complexes each possess only one minimum-energy ligand conformation.

Next, the optimized structures of the rhodium and iridium aldimine complexes were altered by replacing the imine hydrogen atom with several different substituents. The new structures were optimized and the resulting geometries compared. All computed structures (see Table 1) possess a cod ligand for consistency of comparison. With the exception of fluorine there are few non-hydrogen substituents that are less sterically demanding than a methyl group. A flat π-electron system should meet this criterion, *if* the flat plane is oriented normal to the plane of the ligand backbone. The substituents chosen were fluoro, nitro, 3,5-bis(trifluoromethyl)phenyl and phenyl. The optimized structures of $L^{R}Ir(cod)$ where R = F and NO_2 are shown in Figures 11 and 12, respectively. The geometries are discussed in more detail below, but one can see that in the case where R = NO_2, the plane defined by the atoms of R is approximately perpendicular to the ligand backbone.

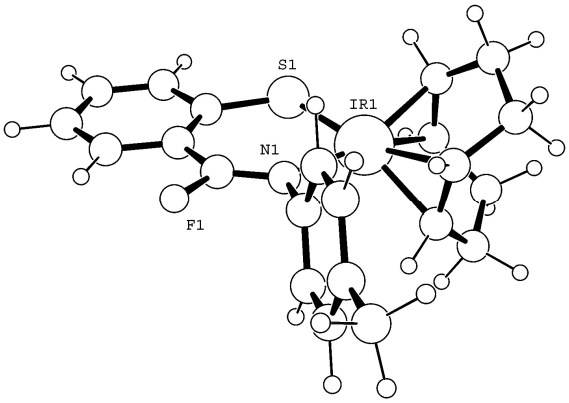

Figure 11. ORTEP diagram of L^RIr(cod) where R = F. Optimized structure at B3LYP/LACVP** level of theory.

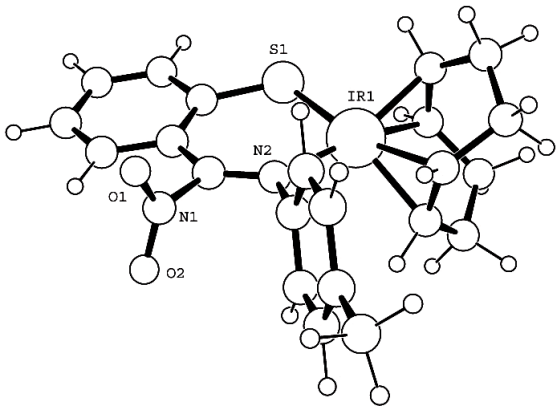

Figure 12. ORTEP diagram of L^RIr(cod) where R = NO_2. Optimized structure at B3LYP/LACVP** level of theory.

Based on electronegativity arguments, the above-mentioned fragments should possess π-electron clouds that increase their spatial protrusion (normal to the plane containing the atomic nuclei) in the order NO_2 < 3,5-$(CF_3)_2$Ph < Ph. That is, a phenyl group should be "thicker" than a nitro group. In order to check this assumption, electron-density isovalue plots were calculated for nitromethane, 3,5-bis(trifluoromethyl)toluene and toluene at the B3LYP/6-311G**++ level of theory and are depicted in Figure 13a (from left to right, respectively). Figure 13b shows two views of all plots superimposed at the methyl carbon. From the top view (left) it can be seen that the toluene π-electron cloud (green) projects above that of 3,5-bis(trifluoromethyl)toluene (blue) throughout the aromatic ring. From the side view (right) in which the electron-density contours of the two aromatic rings have been rendered transparent, one can see that the two aromatic rings are very close in extent. The nitro system, however, is

significantly contracted relative to the other two systems. Thus, it can be assumed that the order of π-cloud extent postulated above is valid with respect to this study, although difference between 3,5-bis(trifluoromethyl)phenyl and phenyl is small.

a

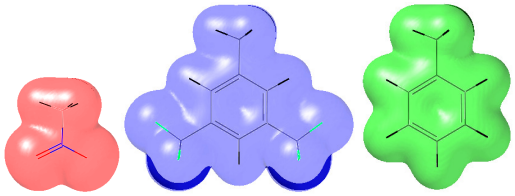

b

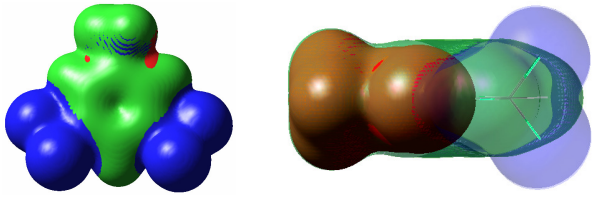

Figure 13a. Electron density isovalues (95%) for nitromethane, 3,5-bis(trifluoromethyl)toluene and toluene, respectively. **b.** Top and side views, respectively, of the three systems superimposed at the methyl carbon. Computed at B3LYP/6-311G**++ level of theory.

Quantitative analysis of the above computations requires a set of parameters that are comparable across the range of structures presented. We define the three parameters **d**, **τ** and **γ** (Chart1). The parameter **d** is defined as the distance from the thiolate sulfur to the imine nitrogen and is a measure of effective metal size. The parameter **τ** is the sum of the two bond angles α and β that share the thiophenylate-imine bond, and is an indirect measure of the distance between the ketimine functionality and the ortho hydrogen of the thiophenylate ring. Finally, **γ** is the torsion angle about the thiophenylate-imine bond which indicates the degree of non-planarity of the ligand backbone. Assuming the geometry about the imine carbon cannot drastically change, if **d** is held constant then an increase in **τ** must be accompanied by an expansion of **γ**. That is, increasing **τ** has the effect of shortening **d** while increasing **γ** lengthens **d** (at the expense π-electron conjugation). Therefore, there should be a threshold region where

steric pressure between R and the ortho hydrogen of the thiophenylate ring overcomes the stabilization energy of π-electron conjugation, causing the ligand to prefer a non-planar geometry.

Chart 1. Structural parameters affecting ligand conformation. $\tau = \alpha + \beta$; ●, ○ = γ_{calc}, γ_{exp}; ■, □ = d_{calc}, d_{exp}).

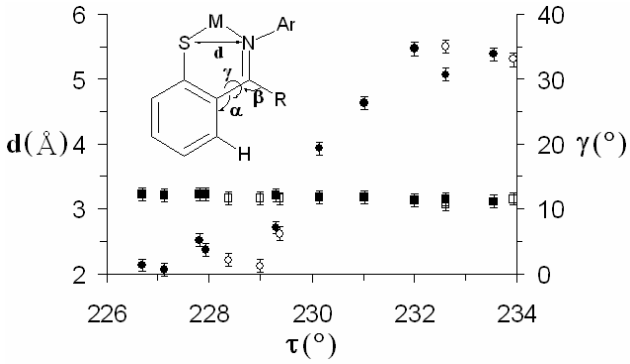

Table 1. Computed and experimental parameters, by ascending **τ** value.[a]

Entry	Method	Ar	R	M	τ (°)	d (Å)	γ (°)
1	DFT[b]	*p*-C_6H_4Me	H	Rh	226.69	3.224	1.3
2	DFT	*p*-C_6H_4Me	H	Ir	227.12	3.215	0.6
3	DFT	*p*-C_6H_4Me	F	Rh	227.82	3.219	5.2
4	DFT	*p*-C_6H_4Me	F	Ir	227.94	3.218	3.7
5(**6**)	XRD	*p*-C_6H_4OMe	H	Ir	228.38	3.166	2.1
6(**5**)	XRD	*p*-C_6H_4OMe	H	Rh	229.00	3.166	1.2
7	DFT	*p*-C_6H_4Me	NO_2	Ir	229.29	3.208	7.1
8(**4**)	XRD	*p*-2,6-$^{i}Pr_2Ph$[c]	H	Ir	229.37	3.155	6.2
9	DFT	*p*-C_6H_4Me	NO_2	Rh	230.15	3.174	19.4
10	DFT	*p*-C_6H_4Me	Ph	Ir	231.03	3.171	26.3
11	DFT	*p*-C_6H_4Me	Ph	Rh	232.01	3.130	34.6
12(**13**)	DFT	*p*-C_6H_4Me	Me	Ir	232.61	3.149	30.7
13(**12**)	XRD	*p*-C_6H_4Me	Me	Rh	232.62	3.062	35.0(7)
14(**12**)	DFT	*p*-C_6H_4Me	Me	Rh	233.55	3.115	33.8
15(**13**)	XRD	*p*-C_6H_4Me	Me	Ir	233.93	3.151	33(1)
16(**10**)	XRD	*p*-C_6H_4Me	Me	H	239.12	2.882	0.2(3)

[a] See Chart 1 for parameter definitions. [b] B3LYP/LACVP**, Jaguar v5.5. [c] 2,6-diisopropylphenyl.

If the region defined above is to be identified, the parameter **d** must remain constant for all values of **τ** and **γ**. Chart 1 shows that **d** is effectively constant for all rhodium and iridium complexes investigated here. The indicated errors in **d** and **γ** are the *largest* estimated errors observed in the experimentally

determined structures and are thus very generous for the majority of data. The errors in τ are probably a significant percentage of the range investigated but should not qualitatively change the outcome. The plot of γ versus τ in Chart 1 shows a trend consistent with the analysis discussed above. All of the aldimine complexes lay to the lower left of the chart, where τ is small and γ is close to zero. Only a slight perturbation in geometry is observed where R = F (entries 3, 4). An increase in τ is observed where R = NO_2, which in the case of M = Ir (entry 7) is accompanied by a slight increase in γ. The γ value where M = Rh (entry 9) is larger, approximately half of the value for the methyl ketimine complexes. The τ parameter increases further where R = Ph (entries 10, 11), and γ is then comparable to those values associated with the methyl ketimines. Again, the rhodium complex exhibits a larger γ value than the analogous iridium complex. The origin of this difference between the complexes of rhodium and iridium is unclear, as they have similar effective metal sizes (see above). From this analysis it is observed that the slight increase in size upon replacing NO_2 with Ph appears to reveal the threshold after which π-conjugation is no longer favored.

Data from computations where R = 3,5-bis(trifluoromethyl)phenyl are not included here. In that case, both planar and bent structures are present within the energy range encompassed by the convergence criteria used in these calculations. Thus it is likely that for this substituent the energy gained through conjugation is nearly exactly counteracted by the energy lost through steric pressure. Also not included in Chart 1 are the optimized structures of $L^RM(cod)$ where R = BH_2 and M = Rh, Ir (Figure 14 where M = Ir). This substituent was included in the study because it is a planar system with no π-electron cloud and thus it should behave as if it were even less sterically demanding than NO_2. While the optimized structures possess planar ligand conformations, they do not conform to the observed trend because the borane fragment is attracted to the π-electron cloud of the nitrogen-bound aryl group and thus τ is increased. Therefore, in this system τ is no longer a viable parameter for comparison with other structures.

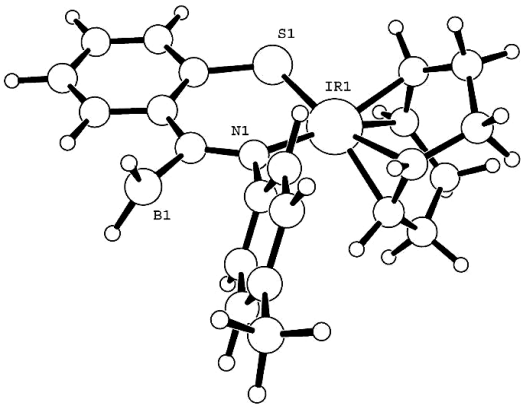

Figure 14. ORTEP diagram of L^RIr(cod) where R = BH_2. Optimized structure at B3LYP/LACVP** level of theory.

Compounds containing nickel or platinum were not included in the study because they possess different **d** values. While **d** is smaller in these systems than in those containing rhodium or iridium, the decrease in size is evidently not great enough for a planar conformation to be realized. The only R = Me case in which planarity is achieved is free ligand **10** (M = H). Here, **τ** can become large enough to accommodate the methyl group because **d** is much smaller than in any case where the ligand binds a metal in a bidentate fashion.

Given that the methyl ketimine complexes appear to prefer a bent ligand conformation, they should either have C_1 symmetry in solution or undergo a ring flip with a low activation barrier. At ambient temperature or above, ^{1}H NMR spectra of **12** and **13** exhibit somewhat broad, featureless cod resonances (Figure 15). These resonances sharpen slightly upon cooling, resolving into complex multiplets that may result from overlapping of non-equivalent peaks (which would be the case for a C_1-symmetric complex). The peak broadening is decidedly small, but is not surprising given the minor change in electronic environment that the cod protons would experience during the ring inversion process. This broadening is not observed in spectra of the analogous (planar) aldimine complexes, a result which supports the conclusion that it is due to a facile ring inversion. Despite efforts to model this process by DFT, no planar transition state could be located using several methods. It is unclear whether the problem is due to an extremely shallow potential energy surface or the presence of a multi-step pathway for ring inversion.

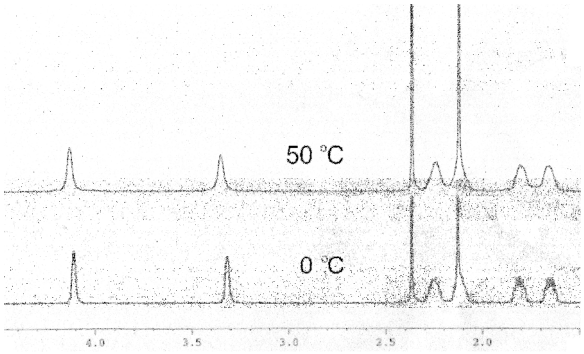

Figure 15. Selected region of the ^{1}H NMR spectrum (ppm) of **12** in CD_2Cl_2, showing broadened cod resonances at 50 °C. Ligand methyl resonances truncated.

Preparation and structures of 3,5-bis(trifluoromethyl)phenyl ketimine complexes. Of the various ligand architectures investigated computationally, the only synthetically accessible ketimine ligand that would (possibly) yield planar metal complexes is that where R = 3,5-bis(trifluoromethyl)phenyl. The diaryl ketone precursor to a ligand of this class was synthesized in a manner analogous to that used for 2-mercaptobenzaldehyde (Scheme 6). Thiocresol was deprotonated with *n*-butyllithium and treated with

Scheme 6.

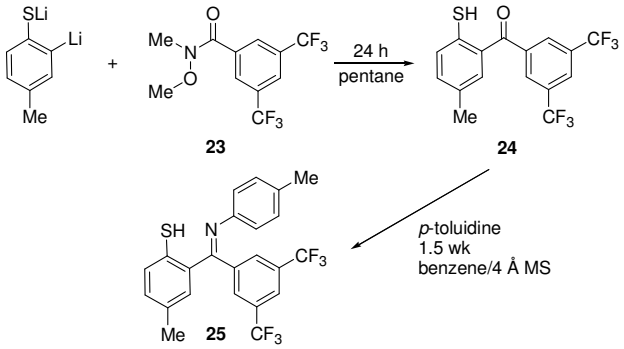

Weinreb amide **23**. The resulting ketone (**24**) was converted to ketimine ligand L^5H (**25**) in good yield by treatment with *p*-toluidine in benzene at ambient temperature. This ligand exhibited reactivity towards metal-complex precursors similar to that of the methyl ketimine analogs discussed above. Thus, $L^5Ni(PPh_3)_2Br$ (**26**), $L^5Pt(PPh_3)_2Cl$ (**27**) and $[L^5Rh(cod)]_2$ (**28**) were prepared by treatment of the appropriate metal complex with L^5K which was generated in situ from **25** (Scheme 7).

Scheme 7.

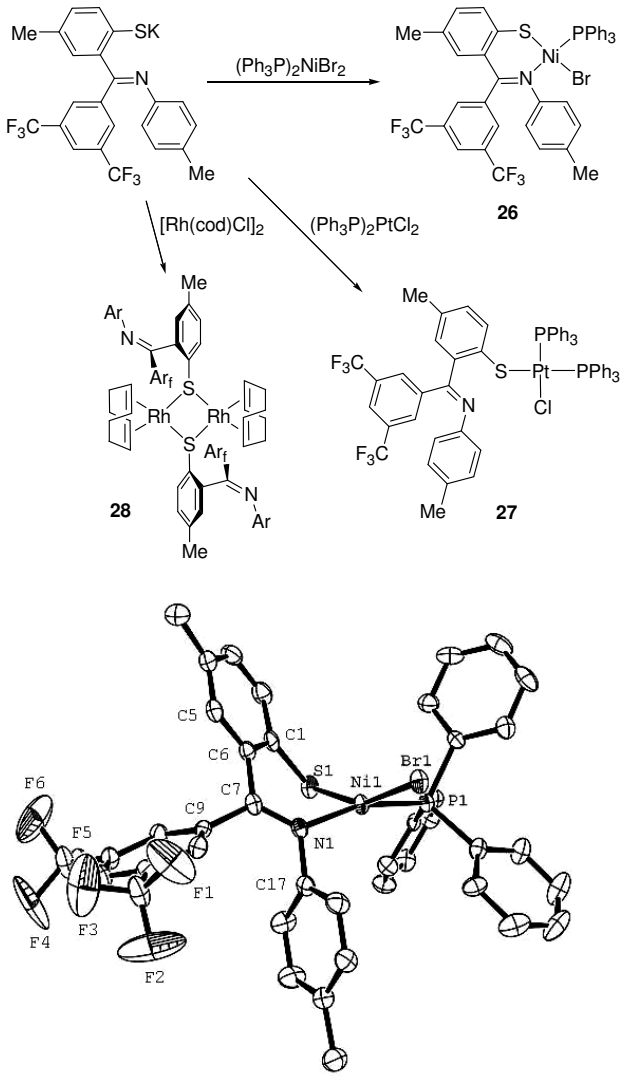

Figure 16. ORTEP diagram of **26** at 50% probability. H atoms omitted for clarity. Selected bond lengths (Å) and angles (°): Ni1-Br1, 2.3554(6); Ni1-S1, 2.169(1); Ni1-P1, 2.157(1); Ni1-N1, 1.940(3); S1-C1, 1.777(4); N1-C7, 1.283(5); C6-C7, 1.464(5); Br1-Ni1-P1, 90.21(3); Br1-Ni1-N1, 96.98(9); S1-Ni1-P1, 90.67(4); S1-Ni1-N1, 89.42(10); C5-C6-C7-C9, 41.6(5).

The solid-state structure of **26** depicted in Figure 16 shows a bent structure similar to those of the methyl ketimine complexes. This datum is inconclusive with respect to the conformational study (see above), as even the nickel aldimine complexes display a variability in ligand conformation. The more informative structures would be the platinum and rhodium complexes. However, unlike the platinum systems containing L^3 or L^4, crystallization of the crude product did not yield $L^5Pt(PPh_3)Cl$. Instead, both phosphine ligands were retained as shown in Figure 17.

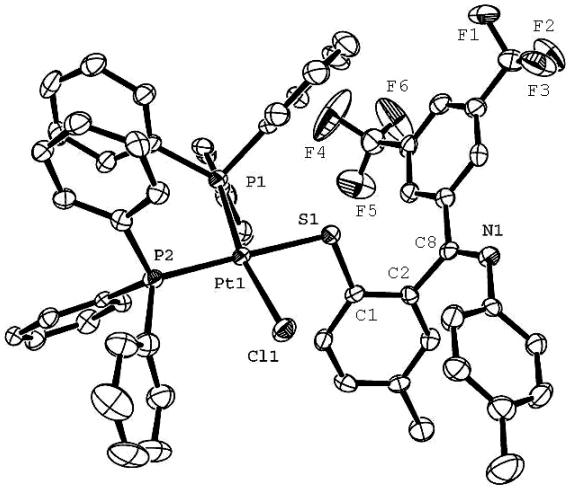

Figure 17. ORTEP diagram of **27** at 50% probability. H atoms omitted for clarity. Selected bond lengths (Å) and angles (°): Pt1-Cl1, 2.338(1); Pt1-S1, 2.362(2); Pt1-P1, 2.253(2); Pt1-P2, 2.281(2); S1-C1, 1.757(6); N1-C8, 1.278(7); C2-C8, 1.503(8); Cl1-Pt1-S1, 88.07(5); Cl1-Pt1-P2, 90.51(5); P1-Pt1-P2, 98.58(6); P1-Pt1-S1, 82.77(5).

X-ray structural investigation of **28** revealed that it is a C_2-symmetric dimer in the solid state, with the thiolate sulfur atoms bridging the rhodium centers (Figure 18). The imine functionalities are both uncoordinated. In solution, **28** is apparently in fast exchange with its monomer and displays highly temperature-dependent NMR resonances (spectra available in Supporting Information). All ^{1}H NMR resonances are broad, and only a single broad peak is observed in the olefinic region. At -80 °C, this region displays many peaks. It is not clear whether these belong to the dimer and monomer or whether more than one isomer of the dimer are present. The broad olefinic peak observed at ambient temperature begins to de-coalesce into two peaks at 70 °C, presumably belonging to the monomer.

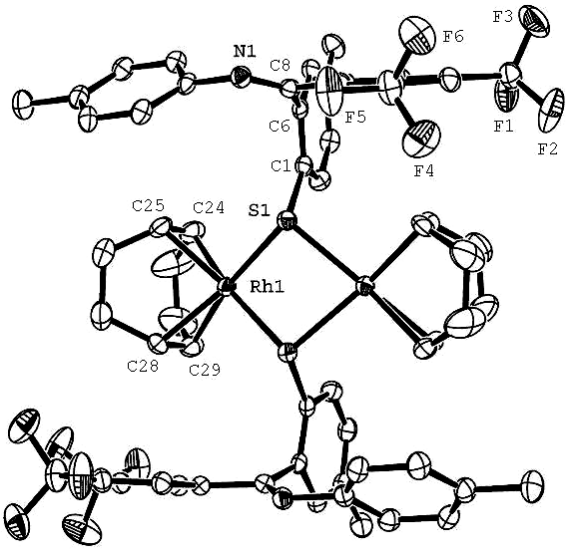

Figure 18. ORTEP diagram of **28** at 50% probability. H atoms omitted for clarity. Selected bond lengths (Å) and angles (°): Rh1-S1, 2.3887(8); Rh1-S1', 2.3801(8); Rh1-C24, 2.147(3); Rh1-C25, 2.148(3); Rh1-C28, 2.140(3); Rh1-C29, 2.137(3); S1-C1, 1.791(3); N1-C8, 1.273(4); C6-C8, 1.510(4); S1-Rh1-S1', 80.64(3); Rh1-S1-Rh1', 94.19(3).

From these data it appears that the electron-withdrawing capabilities of the 3,5-bis(trifluoromethyl)phenyl fragment render the imine nitrogen a poor donor relative to its methyl ketimine analogs. This decrease in donor ability forces the ligand to adopt alternative coordination modes when bound to the heavier platinum group metals. Therefore, the results of the above computational analysis cannot be tested experimentally using this system.

Conclusion

A rational synthesis of thiosalicylaldiminate complexes containing heavy platinum group metals was presented. The ligands were prepared using zinc as a template and metal chlorides were treated with the resulting complexes to yield the target species in moderate to good yield. Iridium species were found to undergo insertion into the imine C-H bond in the presence of strong donor ligands. This reactivity severely limits the potential utility of thiosalicylaldiminates as supporting ligands.

Thiophenoxyketimine analogs were synthesized, which display unexpected coordination behavior. Through computational analysis, the increased steric bulk of the methyl substituent was found to cause significant non-planarity in the ligand backbone, thus reducing π-electron conjugation of the thiophenylate fragment with the imine functionality. The reaction chemistry of these species indicates that their behavior is consistent with the lack of a rigid, conjugated ligand backbone. As imines are generally comparatively poor ligands for heavy, soft metal centers it is therefore of little surprise that the imine functionality of this ligand class should be easily displaced by strongly binding ligands such as phosphines. A corollary to this argument is that the imine substituent would be expected to be much more susceptible to nucleophilic attack than one that is part of a conjugated system such as a β-diketiminate. More study of this new ligand class is needed before any conclusion can be reached concerning their potential utility in catalytic systems.

Experimental Section

General. All manipulations were performed using standard Schlenk-line techniques or an N_2-atmosphere glove box. Reactions followed by NMR spectroscopy were performed in 5 mm Pyrex NMR tubes which were then flame-sealed under reduced pressure. Solvents were dried by passage through a column of activated alumina,[27] degassed with nitrogen and stored over 4 Å molecular sieves. Non-chlorinated solvents were tested with Na/benzophenone prior to use. Deuterated solvents were vacuum-transferred from Na/benzophenone, except CD_2Cl_2 and $CDCl_3$ which were vacuum-transferred from CaH_2. Molecular sieves were activated by heating at 250 °C under high vacuum for 2 d. NMR spectra were obtained with Bruker AMX-300, AMX-400 or DRX-500 spectrometers. Chemical shifts were calibrated relative to residual solvent peaks or external standards and are reported relative to TMS (^{1}H, ^{13}C), 85% H_3PO_4 (^{31}P) and $CFCl_3$ (^{19}F). Infrared spectra were recorded neat on a Thermo Nicolet Avatar 370 spectrometer equipped with a Smart Performer ATR crystal. Elemental analyses were performed at the UC, Berkeley Microanalytical Facility with a Perkin Elmer 2400 Series II CHNO/S Analyzer. All starting materials obtained from commercial sources were used without further purification. 2-Mercaptobenzaldehyde[28] and its sodium salt,[29] copper *tert*-butylsulfide,[30] $[Ir(cod)Cl]_2$,[31] $[Rh(cod)Cl]_2$,[32] $(nbd)PtMe_2$,[33] $(Ph_3P)_2PtMe_2$,[34] $(Me_2S)_2PtCl_2$,[35] $(Ph_3P)_2PtMeCl$,[36] and $(Ph_3P)_2NiPhCl$[37] were prepared according to literature procedures. $Ir(cod)_2Cl$ was prepared by cooling a concentrated solution of $[Ir(cod)Cl]_2$ in neat cod.[38]

Representative Procedure for X-Ray Crystallography. A crystal of appropriate size was mounted on a glass fiber or Kaptan© loop using Paratone-N hydrocarbon oil. The crystal was transferred to a Siemens SMART or APEX diffractometer/CCD area detector,[39] centered in the beam, and cooled by a nitrogen flow low-temperature apparatus that had been previously calibrated by a thermocouple placed at the same position as the crystal. Preliminary orientation matrices and cell constants were determined by collection of 60 10-second frames, followed by spot integration and least-squares refinement. An arbitrary hemisphere of data was collected and the raw data were integrated using SAINT.[40] Cell dimensions reported were calculated from all reflections with $I > 10\ \sigma$. The data were corrected for

Lorentz and polarization effects, but no correction for crystal decay was applied. Data were analyzed for agreement and possible absorption using XPREP.[41] An empirical absorption correction based on comparison of redundant and equivalent reflections was applied using SADABS.[42] The structure was solved and refined with teXsan software package.[43] ORTEP diagrams were created using ORTEP-3 software package.[44]

Table 2a. Crystallographic data for compounds **4** – **6**, **9** and **10**.

Compound #	**4**	**5**	**6**	**9**	**10**
Space Group	$P2_1/n$	$P(-1)$	$P(-1)$	$P(-1)$	$P2_12_12_1$
a, Å	14.4457(9)	8.9880(6)	8.9758(7)	9.4131(7)	7.5851(5)
b, Å	11.3894(7)	10.3914(7)	10.4233(8)	11.4413(9)	11.2611(7)
c, Å	15.7491(9)	11.1130(7)	11.0658(9)	15.924(1)	14.9642(9)
α, deg	90	94.331(1)	93.684(1)	94.483(1)	90
β, deg	112.433(1)	103.799(1)	104.019(1)	89.982(1)	90
γ, deg	90	105.673(1)	106.112(1)	113.337(1)	90
V, Å^3	2395.1(3)	959.6(1)	955.3(1)	1568.9(2)	1278.2(1)
Z	4	2	2	2	4
ρ_{calcd}, g cm^{-3}	1.655	1.569	1.887	1.517	1.254
μ(Mo Kα), mm^{-1}	5.691	1.007	7.127	4.503	0.229
No. rflns measd	12110	5260	4892	8900	7021
No. indep rflns	3446	3160	2643	4336	1444
R_{int}	0.024	0.016	0.038	0.025	0.014
R_1, wR_2[a] (all)	0.0285, 0.0280	0.0261, 0.0311		0.0378, 0.0337	0.0323, 0.0433
R_1, wR_2 (obsd[b])	0.0215, 0.0263	0.0233, 0.0305	0.0383, 0.0485	0.0291, 0.0324	0.0310, 0.0431

[a] $R_1 = \Sigma||F_o| - |F_c||/\Sigma|F_o|$; $wR_2 = [\Sigma\{w(F_o^2 - F_c^2)^2\}/\Sigma w(F_o^2)^2]^{1/2}$. [b] $I > 3.00\sigma(I)$.

Table 2b. Crystallographic data for compounds **12** – **15**, **19**.

Compound #	**12**	**13**	**14**	**15**	**19**
Space Group	$P2_1/c$	$P2_1/c$	$Pbcn$	$P2_1/n$	$P2_1/c$
a, Å	18.801(1)	18.850(2)	22.475(2)	12.0768(8)	8.2563(6)
b, Å	19.655(1)	19.622(2)	14.050(1)	14.864(1)	21.618(2)
c, Å	10.9890(6)	11.0043(9)	17.948(2)	17.228(1)	9.9255(7)
α, deg	90	90	90	90	90
β, deg	106.274(1)	106.214(1)	90	110.004(1)	96.223(1)
γ, deg	90	90	90	90	90
V, Å^3	3898.1(4)	3908.4(5)	5667(1)	2906.0(3)	1761.2(2)
Z	8	8	8	4	4
ρ_{calcd}, g cm^{-3}	1.538	1.838	1.503	1.676	1.873
μ(Mo Kα), mm^{-1}	0.988	6.964	2.253	5.051	8.055
No. rflns measd	17237	16864	25445	13161	8876

No. indep rflns	5274	4300	2868	3517	2538
R_{int}	0.036	0.053	0.077	0.047	0.023
R_1, wR_2 (all)	0.0655, 0.0980	0.0689, 0.0470	0.1213, 0.0955	0.0585, 0.0533	0.0324, 0.0330
R_1, wR_2 (obsd)	0.0524, 0.0853	0.0353, 0.0384	0.0510, 0.0500	0.0334, 0.0375	0.0229, 0.0298

Table2c. Crystallographic data for compounds **26** – **28**.

Compound #	**26**	**27**	**28**
Space Group	$P2_1/c$	$P(-1)$	$C2/c$
a, Å	13.5569(9)	13.492(1)	26.474(1)
b, Å	14.7725(9)	14.743(1)	9.4643(5)
c, Å	22.151(2)	15.712(1)	26.832(1)
α, deg	90	109.336(2)	90
β, deg	91.618(1)	102.825(1)	118.924(1)
γ, deg	90	109.274(2)	90
V, Å^3	4434.4(5)	2583.9(4)	5884.2(5)
Z	4	2	4
ρ_{calcd}, g cm^{-3}	1.454	1.552	1.579
μ(Mo Kα), mm^{-1}	1.486	2.920	0.713
No. rflns measd	22642	15022	15000
No. indep rflns	5358	6612	4220
R_{int}	0.039	0.036	0.020
R_1, wR_2 (all)	0.0652, 0.0537	0.0574, 0.0465	0.0375, 0.0427
R_1, wR_2 (obsd)	0.0396, 0.0476	0.0376, 0.0417	0.0309, 0.0416

Computational Methods. All calculations were performed using the Jaguar 5.5 package[45] with Maestro as the graphical user interface.[46] The hybrid DFT functional B3LYP[47] was used throughout, which consists of the Becke three-parameter functional[48] and the correlation functional of Lee, Yang and Par.[49] The LACVP** basis set was employed,[50] which uses an effective core potential and valence double-ζ contraction basis functions for metals. The remaining atoms are treated with Pople's 6-31G** basis set,[51] which includes a set of *d* polarization functions for non-hydrogen atoms and a set of *p* polarization functions for hydrogens. This level of theory was sufficient to provide optimized structures that agreed quite well with those determined experimentally. All optimized structures converged well employing the DIIS convergence scheme with default convergence criteria. Increasing the size of the SCF grids and the accuracy of the numerical integrations from the default values did not have a

significant effect on the optimized geometries. Vibrational frequencies were calculated for all converged structures and their character as energy minima were confirmed by the absence of negative (imaginary) frequencies. Graphical representations of all computed structures were generated using ORTEP-3. Electron density maps for nitromethane, 3,5-bis(trifluoromethyl)toluene and toluene were computed using the triple-ζ 6-311G**++ basis set[52] which includes diffuse functions on all atoms. Graphical representations were exported directly from Maestro.

2'-*tert*-Butylsulfanylacetophenone. A Schlenk flask was charged with 2'-iodoacetophenone (5.00 g, 20.3 mmol, 1.00 equiv) and copper *tert*-butylsulfide (3.90 g, 25.5 mmol, 1.26 equiv) and flushed with nitrogen gas. Anhydrous DMF (100 mL) was then added via cannula and the reaction mixture was heated at 100 °C for 12 h with stirring in the absence of light. The resulting black solid was allowed to settle and the pale yellow solution decanted into a separatory funnel containing 100 mL H_2O under ambient atmosphere. The gray, opaque suspension was extracted with Et_2O (6 x 50 mL). The Et_2O extracts were then combined, washed with H_2O (4 x 100 mL) and dried over $MgSO_4$. Filtration and removal of the solvent in vacuo yielded a light yellow oil of high purity (4.08 g, 19.6 mmol, 97%). ^{1}H NMR (300 MHz, $CDCl_3$): δ 7.57 (m, 1H), 7.37 (m, 3H), 2.63 (s, 3H), 1.23 (s, 9H). $^{13}C\{^1H\}$ NMR (100.6 MHz, $CDCl_3$): δ 204.90, 148.66, 138.86, 129.74, 129.12, 128.99, 127.05, 47.65, 32.26, 31.03. IR (cm^{-1}): 1693 (s), 1584 (w). Anal. Calcd. for $C_{12}H_{16}OS$: C, 69.19; H, 7.74. Found: C, 68.96; H, 7.69.

***o*-Mercaptoacetophenone.** A Schlenk flask was charged with 4.40 g (33.0 mmol, 1.00 equiv) $AlCl_3$ under nitrogen atmosphere and suspended in 80 mL toluene. The flask was cooled in an IPA/dry ice bath and a solution of 2'-*tert*-butylsulfanylacetophenone (4.00 g, 19.2 mmol, 0.582 equiv) in 20 mL toluene was added via cannula. The reaction mixture was allowed to warm to ambient temperature and was stirred for 20 h. Water (100 mL) was added to the orange suspension, and the mixture was transferred to a separatory funnel under ambient atmosphere. Extraction caused the mixture to become colorless. The organic layer was extracted with 5% aqueous NaOH (4 x 50 mL). All aqueous extracts were then combined and acidified with conc. HCl. The resulting white suspension was extracted with Et_2O (4 x 50 mL) and the Et_2O extracts were combined, washed with H_2O (2 x 50 mL) and dried over $MgSO_4$.

Filtration and removal of the solvent in vacuo resulted in a brown oil which was pure by ^{1}H NMR spectroscopy. Dissolution in CH_2Cl_2 and filtration through a plug of silica removed the brown color, yielding a light yellow oil of similar purity (2.61 g, 17.1 mmol, 92%). ^{1}H NMR (300 MHz, $CDCl_3$): δ 7.89 (d, *J* = 7.5 Hz, 1H), 7.31 (m, 2H), 7.22 (m, 1H), 4.46 (s, 1H), 2.64 (s, 3H). Proton NMR spectra match literature values.[53]

L^1_2Zn (1). Sodium 2-formylbenzenethiolate (400 mg, 2.50 mmol, 1.00 equiv) was suspended in 15 mL of THF. Solid anhydrous $ZnCl_2$ (180 mg, 1.32 mmol, 0.528 equiv) was added and the mixture was stirred for 1 h. 2,6-Diisopropylaniline (448 mg, 2.53 mmol, 1.01 equiv) was then added, followed by 5 g of 4 Å molecular sieves. This mixture was allowed to stand for 2 d, after which time the cloudy solution was filtered and the solvent was removed under vacuum. The residue was dissolved in 5 mL of CH_2Cl_2 and filtered once more. The volume of the resultant yellow solution was reduced to 2 mL and cooled to -30 °C. The supernatant was decanted from the yellow crystalline product that had formed, and the solid was washed with Et_2O (4 x 2 mL) yielding pure **1** (581 mg, 0.882 mmol, 71%). Solvent removal from the supernatant and washes resulted in a residue which, after washing with pentane (5 x 1 mL), yielded an additional 125 mg (0.190 mmol) of **1** of sufficient purity for further use. ^{1}H NMR (500 MHz, CD_2Cl_2): δ 8.17 (s, 2H), 7.28 (br s, 2H), 7.17 (m, 6H), 6.96 (m, 4H), 6.87 (br s, 2H), 3.23 (br s, 2H), 2.67 (br s, 2H), 1.41 (br s, 6H), 1.04 (d, *J* = 6.5 Hz, 12H), 0.60 (br s, 6H). ^{13}C{^{1}H} NMR (125.8 MHz, CD_2Cl_2): δ 173.83, 149.39, 146.97, 142.16 (br), 139.73 (br), 137.32, 136.81, 131.78, 130.62, 127.26, 124.37 (br), 123.09 (br), 122.63, 29.52, 29.28, 25.83, 23.69, 21.64. IR (cm^{-1}): 1620, 1604, 1585, 1541. Anal. Calcd. for $C_{38}H_{44}N_2S_2Zn$: C, 69.33; H, 6.74; N, 4.26. Found: C, 68.99; H, 6.67; N, 4.11.

L^2_2Zn (2). This compound was prepared in the same manner as **1** using sodium 2-formylbenzenethiolate (400 mg, 2.50 mmol, 1.00 equiv), $ZnCl_2$ (170 mg, 1.25 mmol, 0.500 equiv) and *p*-anisidine (308 mg, 2.50 mmol, 1.00 equiv). After dissolution of the crude product in 3 mL CH_2Cl_2, the solution was heated at reflux while 1 mL of pentane was added dropwise (until each drop caused a fleeting cloudiness). Upon cooling to ambient temperature, the homogeneous solution was cooled to -30 °C overnight. The supernatant was decanted and the yellow crystalline solid was washed with Et_2O (3 X

2 mL) (538 mg total, 0.978 mmol, 78%). ^{1}H NMR (500 MHz, CD_2Cl_2): δ 8.21 (s, 2H), 7.57 (d, *J* = 8.0 Hz, 2H), 7.22 (m, 4H), 7.05 (m, 6H), 6.70 (d, *J* = 8.5 Hz, 4H), 3.73 (s, 6H). ^{13}C{^{1}H} NMR (125.8 MHz, CD_2Cl_2): δ 171.15, 159.23, 150.17, 143.46, 139.51, 137.03, 131.98, 130.18, 123.84, 122.67, 114.57, 55.95. IR (cm^{-1}): 1610, 1582, 1537, 1504. Anal. Calcd. for $C_{28}H_{24}N_2O_2S_2Zn$: C, 61.14; H, 4.40; N, 5.09. Found: C, 61.13; H, 4.37; N, 5.03.

L^{1}Rh(cod) (3). A solution of **1** (200 mg, 0.304 mmol, 1.00 equiv) in 5 mL of THF was slowly added to $[Rh(cod)Cl]_2$ (150 mg, 0.304 mmol, 1.00 equiv) dissolved in 12 mL of THF. After stirring the reaction mixture for 4 h the solvent was removed under vacuum. The residue was extracted with Et_2O (4 x 5 mL) and the filtered extracts were combined and reduced to 10 mL. The solution was held at -30 °C for 24 h, resulting in the precipitation of 252 mg (0.496 mmol, 82%) of pure **3**. ^{1}H NMR (500 MHz, CD_2Cl_2): δ 8.19 (d, *J* = 2.5 Hz, 1H), 7.83 (d, *J* = 7.5 Hz, 1H), 7.34 (t, *J* = 7.5 Hz, 1H), 7.25 (m, 3H), 7.09 (t, *J* = 7.5 Hz, 1H), 4.48 (m, 2H), 3.49 (m, 2H), 3.35 (sept, *J* = 7.0 Hz, 2H), 2.32 (m, 4H), 2.02 (m, 2H), 1.90 (m, 2H), 1.40 (d, *J* = 7.0 Hz, 6H), 1.02 (d, *J* = 7.0 Hz, 6H). ^{13}C{^{1}H} NMR (125.8 MHz, CD_2Cl_2): δ 167.96, 149.82, 140.87, 138.11, 132.68, 131.93, 130.11, 127.56, 124.18, 123.90, 122.65, 86.50, 78.23, 30.96, 30.53, 28.74, 25.72, 22.63. IR (cm^{-1}): 1590, 1572, 1524. Anal. Calcd. for $C_{27}H_{34}NRhS$: C, 63.90; H, 6.75; N, 2.76. Found: C, 63.92; H, 6.55; N, 2.72.

L^{1}Ir(cod) (4). This compound was prepared in the same way as **3** using **1** (100 mg, 0.152 mmol, 1.00 equiv) in 5 mL of THF and $Ir(cod)_2Cl$ (135 mg, 0.304 mmol, 2.00 equiv) in 10 mL of THF. The crude product was dissolved in 10 mL of Et_2O, filtered and concentrated to 2 mL with heating. Red crystalline material precipitated upon cooling of the solution to -30 °C. The supernatant was decanted and the solid was washed with pentane (3 x 1 mL) (131 mg, 0.219 mmol, 72%). Crystals of sufficient quality for X-ray diffraction analysis were obtained by cooling of a more dilute solution of **4** in Et_2O. ^{1}H NMR (500 MHz, CD_2Cl_2): δ 8.66 (s, 1H), 7.99 (d, *J* = 8.5 Hz, 1H), 7.54 (m, 2H), 7.30 (m, 3H), 7.12 (m, 1H), 4.29 (m, 2H), 3.18 (sept, *J* = 7.0 Hz, 2H), 3.00 (m, 2H), 2.12 (m, 4H), 1.91 (m, 2H), 1.77 (m, 2H), 1.34 (d, *J* = 6.5 Hz, 6H), 1.00 (d, *J* = 6.5 Hz, 6H). ^{13}C{^{1}H} NMR (125.8 MHz, CD_2Cl_2): δ 165.93, 149.03, 148.53,

141.23, 138.16, 132.50, 132.25, 130.19, 127.99, 123.98, 122.68, 69.29, 62.50, 31.78, 30.62, 28.55, 25.71, 22.66. IR(cm^{-1}): 1595, 1572, 1526. Anal. Calcd. for $C_{27}H_{34}IrNS$: C, 54.33; H, 5.74; N, 2.35. Found: C, 54.19; H, 5.95; N, 2.25.

L^2Rh(cod) (5). A solution of **2** (129 mg, 0.234 mmol, 1.00 equiv) in 5 mL of THF was slowly added to $[Rh(cod)Cl]_2$ (116 mg, 0.235 mmol, 1.00 equiv) dissolved in 10 mL of THF. After stirring the reaction mixture for 6 h the solvent was removed under vacuum. The residue was extracted with 3 mL of CH_2Cl_2, filtered, and heated to boiling while 2 mL of pentane was added. The vessel was then cooled to -30 °C overnight. The supernatant was decanted and the orange solid was washed with Et_2O (3 x 1 mL) (204 mg, 0.450 mmol, 96%). Crystals suitable for X-ray diffraction analysis were grown by vapor diffusion of pentane into a solution of **5** in THF. ^{1}H NMR (500 MHz, THF-d_8): δ 8.39 (s, 1H), 7.72 (d, *J* = 8.0 Hz, 1H), 7.46 (d, *J* = 6.5 Hz, 1H), 7.22 (m, 1H), 7.07 (d, *J* = 8.5 Hz, 2H), 6.96 (m, 1H), 6.89 (d, *J* = 8.5 Hz, 2H), 4.37 (br s, 2H), 3.78 (s, methyl and cod olefinic overlapping, 5H), 2.27 (m, 4H), 1.95 (br s, 2H), 1.85 (br s, 2H). ^{13}C{^{1}H} NMR (125.8 MHz, THF-d_8): δ 168.61, 158.84, 151.46, 149.23, 138.51, 132.45, 131.43, 130.47, 125.28, 121.70, 114.25, 84.35, 76.85, 55.79, 31.36, 30.90. IR (cm^{-1}): 1605, 1590, 1574, 1523. Anal. Calcd. for $C_{22}H_{24}NORhS$: C, 58.28; H, 5.34; N, 3.09. Found: C, 58.14; H, 5.21; N, 3.15.

L^2Ir(cod) (6). A solution of **2** (200 mg, 0.364 mmol, 1.00 equiv) in 5 mL of THF was slowly added to a solution of 322 mg (0.364 mmol, 1.00 equiv) of $[Ir(cod)Cl]_2$·2cod (from $Ir(cod)_2Cl$) in 10 mL of THF, and the reaction mixture was stirred for 6 h. After removal of the solvent, the residue was extracted with 10 mL of CH_2Cl_2 leaving behind an unidentified yellow substance. The extract was reduced to 2 mL and cooled to -30 °C overnight. The supernatant was then decanted and the deep red, microcrystalline solid was washed with Et_2O (3 x 1 mL) (108 mg, 0.199 mmol, 27%). ^{1}H NMR (400 MHz, CD_2Cl_2): δ 8.37 (s, 1H), 7.96 (d, *J* = 8.0 Hz, 1H), 7.54 (d, *J* = 8.0 Hz, 1H), 7.50 (t, *J* = 7.5 Hz, 1H), 7.11 (t, *J* = 7.5 Hz, 1H), 7.07 (d, *J* = 8.8 Hz, 2H), 6.92 (d, *J* = 8.8 Hz, 2H), 4.27 (m, 2H), 3.83 (s, 3H), 3.37 (m, 2H), 2.13 (m, 4H), 1.88 (m, 2H), 1.75 (m, 2H). ^{13}C{^{1}H} NMR (125.8 MHz, CD_2Cl_2): δ 166.34, 158.43, 148.26,

147.64, 138.34, 132.34, 132.06, 130.23, 125.39, 122.52, 113.61, 67.71, 62.21, 56.02, 31.62, 30.64. IR (cm^{-1}): 1603, 1594, 1568, 1523, 1500. Anal. Calcd. for $C_{22}H_{24}IrNOS$: C, 48.69; H, 4.46; N, 2.58. Found: C, 48.76; H, 4.51; N, 2.54.

(L^1-H)Ir(PMe_3)$_3$H (9). Compound **4** (73.5 mg, 0.123 mmol, 1.00 equiv) was dissolved in 1 mL of benzene and 0.70 mmol (5.7 equiv) of trimethylphosphine was added via vacuum transfer. The reaction mixture was then heated at 65 °C for 1 h. The solvent and excess phosphine were removed under reduced pressure, and the residue was dissolved in 1 mL of CH_2Cl_2. Crystalline material was obtained by slow vapor diffusion of pentane (2 mL) into the CH_2Cl_2 solution (64.5 mg, 0.0900 mmol, 73%). ^{1}H NMR (500 MHz, CD_2Cl_2) δ 7.26 (d, J = 7.0 Hz, 1H), 7.03 (m, 1H), 6.91 (m, 1H), 6.78 (m, 1H), 6.65 (m, 2H), 6.15 (t, J = 7.0 Hz, 1H), 3.27 (sept, J = 7.0 Hz, 1H), 2.91 (sept, J = 7.0 Hz, 1H), 1.76 (d, $J_{H\text{-}P}$ = 10 Hz, 9H), 1.65 (d, $J_{H\text{-}P}$ = 8.0 Hz, 9H), 1.36 (d, $J_{H\text{-}P}$ = 8.5 Hz, 9H), 1.22 (d, J = 7.0 Hz, 3H), 1.13 (d, J = 7.0 Hz, 3H), 1.01 (d, J = 7.0 Hz, 3H), 0.47 (d, J = 7.0 Hz, 3H), -11.22 (d of t, $J_{H\text{-}P}$ = 191 Hz, 22.5 Hz, 1H). ^{13}C{^{1}H} NMR (100.6 MHz, CD_2Cl_2): δ 190-185 (m), 156.66, 154.15, 151.01, 136.21, 133.86, 127.99, 127.66, 127.53, 124.38, 123.17, 120.29, 118.40, 28.44 (d, $J_{C\text{-}P}$ = 49 Hz), 25.32 (d, $J_{C\text{-}P}$ = 25 Hz), 23.71 (d, $J_{C\text{-}P}$ = 36 Hz), 22.22, 21.94, 21.79, 21.42, 17.28, 17.01. ^{31}P{^{1}H} NMR (162.0 MHz, CD_2Cl_2): δ -44.65 (m), -58.58 (m), -63.80 (m). IR (cm^{-1}): 2026, 1579, 1545. Anal. Calcd. for $C_{28}H_{49}IrNP_3S$: C, 46.91; H, 6.89; N, 1.95. Found: C, 47.16; H, 6.96; N, 1.93.

L^3H (10). *o*-Mercaptoacetophenone (591 mg, 3.88 mmol, 1.00 equiv) was diluted with 15 mL of benzene and *p*-toluidine (416 mg, 3.88 mmol, 1.00 equiv) was added, followed by 5 g of 3 Å molecular sieves. The reaction mixture was allowed to stand for 2 days, during which time the solution became deep red. After solvent removal the resulting amorphous powder was dissolved in 3 mL of THF and gently heated. During heating, pentane (15 mL) was slowly added, resulting in the formation of bright red crystals upon cooling. The reaction vessel was then placed in a -30 °C freezer overnight. The supernatant was removed, and the crystalline material (791 mg, 3.28 mmol, 84%) was washed with pentane. Note: the crude product was pure by ^{1}H NMR and could be used without purification. Crystals suitable for X-ray crystallographic analysis were grown by cooling a concentrated solution of **10** in

Et_2O. ^1H NMR (500 MHz, CD_2Cl_2): δ 17.33 (s, 1H), 7.74 (d, *J* = 1.5 Hz, 1H), 7.72 (d, *J* = 1.0 Hz, 1H), 7.31 (d, *J* = 8.0 Hz, 2H), 7.13 (m, 3H), 6.98 (m, 1H), 2.55 (s, 3H), 2.41 (s, 3H). $^{13}C\{^1H\}$ NMR (125.8 MHz, CD_2Cl_2): δ 172.08, 162.19, 138.35, 138.32, 136.57, 131.97, 130.57, 130.53, 128.11, 124.37, 121.36, 21.37, 18.40. IR (cm^{-1}): 1615, 1585, 1531. Anal. Calcd. for $C_{15}H_{15}NS$: C, 74.65; H, 6.26; N, 5.80. Found: C, 74.47; H, 6.41; N, 5.76.

L^4H (11). *o*-Mercaptoacetophenone (485 mg, 3.19 mmol, 1.00 equiv) was diluted with 10 mL of benzene and *p*-anisidine (395 mg, 3.21 mmol, 1.01 equiv) was added, followed by 3 g of 3 Å molecular sieves. The reaction mixture was allowed to stand for 2 days, during which time the solution became deep red. The mixture was then filtered through a plug of neutral alumina and lyophilized, yielding a red amorphous powder. The powder was dissolved in 3 mL of CH_2Cl_2 and heated while 5 mL of pentane was slowly added. Bright red needles formed upon cooling to room temperature. The reaction vessel was then placed in a -30 °C freezer overnight. The supernatant was removed, and the crystals were washed with Et_2O (3 x 2 mL), yielding 590 mg of product. The Et_2O washes were added to the supernatant, which resulted in an additional crop of crystals (76 mg) after cooling at -30 °C for 2 days (666 mg total, 2.59 mmol, 81%). ^1H NMR (500 MHz, CD_2Cl_2): δ 18.17 (s, 1H), 7.74 (d, *J* = 1.5 Hz, 1H), 7.72 (d, *J* = 1.5 Hz, 1H), 7.19 (m, 2H), 7.12 (m, 1H), 7.02 (m, 2H), 6.96 (m, 1H), 3.85 (s, 3H), 2.58 (s, 3H). $^{13}C\{^1H\}$ NMR (125.8 MHz, CD_2Cl_2): δ 172.44, 164.23, 159.77, 138.86, 132.11, 131.01, 130.52, 127.52, 126.14, 121.04, 115.23, 56.13, 18.31. IR (cm^{-1}): 1607, 1582, 1506. Anal Calcd. for $C_{15}H_{15}NOS$: C, 70.00; H, 5.87; N, 5.44. Found: C, 70.01; H, 6.01; N, 5.43.

L^3Rh(cod) (12). Yellow $[Rh(cod)Cl]_2$ (203 mg, 0.412 mmol, 1.00 equiv) was dissolved in 10 mL of THF and cooled to -30 °C. Ligand **10** (200 mg, 0.829 mmol, 2.01 equiv) was dissolved in 4 mL of THF, and NaH (21.3 mg, 0.843 mmol) was added, causing vigorous gas evolution. After 30 min the solution had become light yellow, at which time it was slowly added to the cooled $[Rh(cod)Cl]_2$ solution. The mixture was allowed to stir for 4 h, and the solvent was removed under vacuum. ^1H NMR spectra showed quantitative conversion to product. The residue was dissolved in 3 mL CH_2Cl_2, filtered, and the solution was gently heated while 10 mL of pentane was slowly added. The reaction vessel was placed in

a -30 °C freezer overnight. The supernatant was removed from the resulting orange crystalline material and the solid was washed with pentane (342 mg, 0.758 mmol, 92%). Slow evaporation of a CH_2Cl_2 solution of **12** yielded crystals of sufficient quality for X-ray diffraction analysis. ^{1}H NMR (500 MHz, CD_2Cl_2): δ 7.62 (d, *J* = 7.5 Hz, 1H), 7.45 (d, *J* = 8.0 Hz, 1H), 7.21 (d, *J* = 8.0 Hz, 2H), 7.08 (m, 1H), 6.99 (m, 1H), 6.91 (d, *J* = 8.0 Hz, 2H), 4.14 (br s, 2H), 3.35 (br s, 2H), 2.38 (s, 3H), 2.27 (br s, 2H), 2.14 (br s, methyl and cod methylene overlapping, 5H), 1.81 (br s, 2H), 1.67 (br s, 2H). ^{13}C{^{1}H} NMR (125.8 MHz, CD_2Cl_2): δ 171.42, 148.67, 147.40, 138.44, 135.71, 132.66, 131.26, 129.90, 129.82, 122.28, 121.84, 86.23 (d, $J_{C\text{-}Rh}$ = 10.1 Hz), 76.68 (d, $J_{C\text{-}Rh}$ = 12.6 Hz), 31.46, 30.59, 24.31, 21.21. IR (cm^{-1}): 1958, 1933, 1903, 1582, 1565, 1534, 1504. Anal. Calcd. for $C_{23}H_{26}NRhS$: C, 61.19; H, 5.80; N, 3.10. Found: C, 61.11; H, 5.95; N, 3.18.

L^{3}Ir(cod) (13). A solution of $[Ir(cod)Cl]_2$·2cod was prepared by dissolution of $Ir(cod)_2Cl$ (368 mg, 0.829 mmol, 1.00 equiv) in 15 mL of THF. Ligand **10** (200 mg, 0.829 mmol, 1.00 equiv) was dissolved in 5 mL of THF, and NaH (20.0 mg, 0.835 mmol, 1.01 equiv) was added. After allowing the reaction mixture to stir for 30 min the resulting yellow solution was slowly added to the $[Ir(cod)Cl]_2$·2cod solution, causing a color change from orange to deep red. The mixture was stirred for 4 h, after which time the solvent was removed under vacuum. The dark residue was then dissolved in 4 mL of CH_2Cl_2, filtered, and gently heated while 5 mL of Et_2O was slowly added. Upon cooling to ambient temperature, a small quantity of black precipitate formed. This was filtered off and the homogeneous solution was stored at -30 °C overnight. The supernatant was decanted and the cherry red precipitate was washed with Et_2O (3 x 1 mL) to yield 162 mg (0.300 mmol, 36%) of pure **13**. Attempts to recover a second crop of product by the above method were unsuccessful, as an unidentified orange substance precipitated with the desired product. However, a small crop (25.5 mg, 0.0472 mmol) of **13** was isolated by cooling a THF solution (3 mL) of the material present in the supernatant after addition of 4 mL of Et_2O. Crystals of a quality suitable for X-ray diffraction analysis were grown by slow diffusion of pentane into a CH_2Cl_2 solution of purified **13**. ^{1}H NMR (500 MHz, CD_2Cl_2): δ 7.76 (d, *J* = 8.0 Hz, 1H), 7.65 (d, *J* = 8.0 Hz, 1H), 7.24 (d, *J* = 8.0 Hz, 2H), 7.19 (t, *J* = 8.0 Hz, 1H), 7.04 (t, *J* = 8.0 Hz, 1H), 6.88 (d, *J* = 8.0

Hz, 2H), 4.00 (br s, 2H), 2.90 (br s, 2H), 2.43 (s, 3H), 2.24 (s, 3H), 2.09 (br s, 2H), 2.00 (br s, 2H), 1.68 (br s, 2H), 1.51 (br s, 2H). $^{13}C\{^{1}H\}$ NMR (125.8 MHz, CD_2Cl_2): δ 170.98, 148.45, 146.37, 136.15, 135.64, 132.24, 132.17, 130.36, 129.44, 123.23, 122.40, 68.76, 61.80, 31.46, 25.44, 21.16. IR (cm^{-1}): 1585, 1560, 1525, 1504. Anal. Calcd. for $C_{23}H_{26}IrNS$: C, 51.09; H, 4.85; N, 2.59. Found: C, 51.44; H, 4.91; N, 2.56.

$L^3Ni(PPh_3)Br$ (14). NaH (4.84 mg, 0.202 mmol, 1.00 equiv) was added to a solution of **10** (48.7 mg, 0.206 mmol, 1.02 equiv) in 5 mL of THF. The mixture was stirred for 30 min during which time its color changed from deep red to light yellow. This solution was then added dropwise to a solution of $(Ph_3P)_2NiBr_2$ (150 mg, 0.202 mmol, 1.00 equiv) in 10 mL of THF and stirred overnight. The solvent was removed under reduced pressure, and the residue was extracted with 3 mL of CH_2Cl_2 and filtered. While heating at reflux, hexane (15 mL) was slowly added. Dark brown product precipitated upon cooling. This material was then washed with Et_2O (3 x 2 mL) (105 mg, 0.164 mmol, 81%). Recrystallization from CH_2Cl_2/pentane yielded crystals suitable for X-ray diffraction analysis. ^{1}H NMR (400 MHz, CD_2Cl_2): δ 7.72 (m, 6H), 7.59 (dd, *J* = 7.6, 1.2 Hz, 1H), 7.52 (m, 4H), 7.37 (m, 10H), 7.20 (t, *J* = 7.2 Hz, 1H), 7.09 (t, *J* = 7.2 Hz, 1H), 2.67 (s, 3H), 2.12 (s, 3H). $^{13}C\{^{1}H\}$ NMR (125.8 MHz, CD_2Cl_2): δ 167.99, 146.32, 143.76, 137.81, 137.43, 135.92, 135.27, 132.40, 130.76, 130.51, 129.27, 128.92, 128.30, 126.40, 125.28, 23.31, 21.09. IR (cm^{-1}): 1597, 1584, 1541, 1503. Anal. Calcd. for $C_{33}H_{29}BrNNiPS \cdot 0.25CH_2Cl_2$: C, 60.20; H, 4.48; N, 2.11. Found: C, 60.70; H, 4.46; N, 2.10.

$L^3Pt(PPh_3)Cl$ (15). NaH (9.98 mg, 0.416 mmol, 1.00 equiv) was added to a solution of **10** (100 mg, 0.414 mmol, 0.995 equiv) in 5 mL of THF. The mixture was stirred for 30 min and was then added dropwise to a suspension of $(Ph_3P)_2PtCl_2$ (326 mg, 0.413 mmol, 0.993 equiv) in 10 mL of THF and stirred overnight. The solvent was removed under reduced pressure, and the residue was extracted with 10 mL of benzene and lyophilized. The crude product was allowed to stand under 10 mL of Et_2O for 2 weeks, and the Et_2O was then decanted. This process was then repeated, after which time the remaining solid was extracted with 2 mL of THF. Vapor diffusion of pentane (1 mL) into this solution resulted in crystalline **15** (64.5 mg, 0.0880 mmol, 21%). ^{1}H NMR (500 MHz, CD_2Cl_2): δ 7.62 (m, 6H), 7.52 (d, *J* =

7.0 Hz, 1H), 7.44 (m, 3H), 7.37 (m, 6H), 7.29 (m, 5H), 7.14 (m, 2H), 2.44 (s, 3H), 2.28 (s, 3H). $^{13}C\{^{1}H\}$ NMR (125.8 MHz, CD_2Cl_2): δ 171.32, 146.93, 141.46 (d, $J_{C\text{-}P}$ = 6.3 Hz), 136.73, 135.10 (d, $J_{C\text{-}P}$ = 11.3 Hz), 132.17, 131.23, 131.15, 130.55, 130.30, 129.79, 129.42, 128.40 (d, $J_{C\text{-}P}$ = 11.3 Hz), 125.13, 124.80, 23.53, 21.38. $^{31}P\{^{1}H\}$ NMR (162 MHz, CD_2Cl_2): δ 12.02 ($J_{P\text{-}Pt}$ = 3914 Hz). IR (cm^{-1}): 1594, 1552, 1505. Anal. Calcd. for $C_{33}H_{29}ClNPPtS$: C, 54.06; H, 3.99; N, 1.91. Found: C, 53.70; H, 3.81; N, 1.82. Compound **16**, present in the crude reaction mixture, was not obtained in analytically pure form. NMR spectra of **16** are available as Supporting Information.

$L^4Pt(PPh_3)Cl$ (17) and $L^4Pt(PPh_3)_2Cl$ (18). Potassium *tert*-butoxide (43.1 mg, 0.384 mmol, 1.00 equiv) was added to a solution of **11** (97.7 mg, 0.380 mmol, 0.989 equiv) in 5 mL of THF, resulting in a color change from deep red to light orange. A Schlenk flask was charged with $(Ph_3P)_2PtCl_2$ (300 mg, 0.380 mmol, 0.989 equiv) and 100 mL of THF. The vessel was cooled in an IPA/dry ice bath, and the L^4K solution was slowly added via cannula. The reaction mixture was stirred and allowed to warm to ambient temperature over 4 h, after which time the solvent was removed under vacuum. The residue was extracted with benzene (10 mL) and lyophilized to yield an amorphous light orange powder, to which 10 mL of Et_2O was then added. After 12 h all of the amorphous powder was converted to pure, crystalline **17** (220 mg, 0.294 mmol, 77%). Some crystals obtained by the above procedure were suitable for X-ray diffraction analysis. Note: When the reaction was performed at ambient temperature and/or higher concentration, compound **18** was also formed, although this compound was not successfully isolated. Data are for **17** only. ^{1}H NMR (500 MHz, CD_2Cl_2): δ 7.59 (m, 6H), 7.52 (m, 1H), 7.43 (m, 3H), 7.36 (m, 6H), 7.31 (d, J = 9.0 Hz, 2H), 7.26 (m, 1H), 7.13 (m, 2H), 6.99 (d, J = 9.0 Hz, 2H), 3.86 (s, 3H), 2.28 (s, 3H). $^{13}C\{^{1}H\}$ NMR (125.8 MHz, CD_2Cl_2): δ 171.64, 158.53, 141.45 (d, $J_{C\text{-}P}$ = 3.8 Hz), 135.11 (d, $J_{C\text{-}P}$ = 10.1 Hz), 132.16, 131.23, 131.16, 130.58, 130.32, 129.82, 128.40 (d, $J_{C\text{-}P}$ = 11.3 Hz), 126.34, 124.80, 113.92, 55.96, 23.51. $^{31}P\{^{1}H\}$ NMR (202.4 MHz, CD_2Cl_2): δ 10.66 ($J_{P\text{-}Pt}$ = 3903 Hz). IR (cm-1): 1605, 1585, 1561, 1503. Anal. Calcd. for $C_{33}H_{29}ClNOPPtS$: C, 52.91; H, 3.90; N, 1.87. Found: C, 53.23; H, 4.02; N, 1.92.

[$L^4PtMe_3]_2$ (19). A solution of **11** (40.0 mg, 0.155 mmol, 1.00 equiv) in 3 mL of acetonitrile was slowly added to 49.5 mg (0.156 mmol, 1.01 equiv) of (nbd)$PtMe_2$ in 5 mL of acetonitrile. The mixture quickly developed a dark orange color, then turned light orange after ca. 5 min. After 6 h, a brick red precipitate had formed which was collected by filtration and washed with acetonitrile (3 x 1 mL). This sparingly soluble material was not successfully purified although its ^{1}H NMR spectrum is consistent with the crystallographically determined structure (see Supporting Information). The supernatant from the reaction mixture was allowed to stand for 2 d, during which time a few high-quality crystals formed which were used for the X-ray structural determination.

$L^3Rh(P(p\text{-tol})_3)_2$ (20). Tri(*p*-tolyl)phosphine (135 mg, 0.444 mmol, 1.00 equiv) was added to a solution of **12** (100 mg, 0.222 mmol, 0.500 equiv) dissolved in 10 mL of benzene, causing a rapid color change from orange to dark purple/red. The reaction mixture was stirred for 24 h, after which time the solvent was removed under reduced pressure. The residue was dissolved in 2 mL of THF and heated to boiling while 12 mL of hexane was slowly added. Upon cooling to ambient temperature, the vessel was cooled at -30 °C for 24 h. The supernatant was decanted and the dark purple solid was washed with Et_2O (3 x 2 mL) (167 mg, 0.175 mmol, 79%). ^{1}H NMR (500 MHz, CD_2Cl_2): δ 7.64 (d, J = 7.5 Hz, 1H), 7.41 (m, 6H), 7.28 (d, J = 7.5 Hz, 1H), 7.23 (m, 1H), 7.10 (t, J = 7.5 Hz, 1H), 7.07 (d, J = 8.0 Hz, 2H), 6.90 (m, 12H), 6.80 (m, 6H), 6.35 (br s, 2H), 2.46 (s, 3H), 2.32 (s, 9H), 2.29 (s, 9H), 1.92 (s, 3H). ^{13}C{^{1}H} NMR (125.8 MHz, CD_2Cl_2): δ 169.75, 149.06, 146.33, 138.82, 138.66, 135.16, 135.02, 134.93, 134.69, 134.32, 134.22, 133.88, 133.58, 132.89, 130.20, 128.79, 128.06, 127.98, 127.45, 123.92, 121.82, 21.78, 21.56, 21.50, 21.29. ^{31}P{^{1}H} NMR (162.0 MHz, CD_2Cl_2): δ 46.51 (dd, $J_{P\text{-}P}$ = 42.1 Hz, $J_{P\text{-}Rh}$ = 179.8 Hz), 40.02 (dd, $J_{P\text{-}P}$ = 42.1 Hz, $J_{P\text{-}Rh}$ = 183.1 Hz). IR (cm^{-1}): 1598, 1578, 1539. Anal. Calcd. for $C_{57}H_{56}NP_2RhS$: C, 71.92; H, 5.93; N, 1.47. Found: C, 70.91; H, 6.02; N, 1.41. Analysis of two independently prepared and purified samples showed similarly low abundance of carbon. NMR spectra of pure **20** are available as Supporting Information.

Weinreb amide 23. A round-bottomed flask was charged with 10.7 g (38.7 mmol, 1.00 equiv) 3,5-bis(trifluoromethyl)benzoyl chloride and flushed with N_2. Ethanol-free chloroform (200 mL) was added,

followed by *N,O*-dimethylhydroxylamine hydrochloride (4.16 g, 42.6 mmol, 1.10 equiv). The reaction mixture was stirred under an N_2 until a homogeneous solution was obtained (gentle heating was needed), then the flask was cooled in an ice bath. Pyridine (7.3 mL, 90 mmol, 2.3 equiv) was slowly added via syringe causing the evolution of a colorless vapor. The flask was allowed to warm to room temperature and the reaction mixture was stirred for 4 h. An Et_2O/CH_2Cl_2 mixture (1:1 by volume, 100 mL) was added, and the solution was extracted with water (6 x 50 mL) then brine (50 mL). The organic portion was dried over $MgSO_4$ and filtered. Removal of the solvent under vacuum yielded pure **23** (11.1 g, 36.8 mmol, 95%). ^{1}H NMR (500 MHz, CD_2Cl_2): δ 8.20 (s, 2H), 8.00 (s, 1H), 3.54 (s, 3H), 3.38 (s, 3H). $^{13}C\{^1H\}$ NMR (125.8 MHz, CD_2Cl_2): δ 166.87, 136.81, 131.84 (q, $J_{C\text{-}F}$ = 34.0 Hz), 129.42, 124.74 (quint., $J_{C\text{-}F}$ = 3.8 Hz), 123.75 (q, $J_{C\text{-}F}$ = 273.0 Hz), 61.94, 33.54. ^{19}F NMR (376.5 MHz, CD_2Cl_2): δ -62.52. IR (cm^{-1}): 1655, 1620, 1426, 1392, 1356. Anal. Calcd. for $C_{11}H_9F_6NO_2$: C, 43.87; H, 3.01; N, 4.65. Found: C, 44.13; H, 2.95; N, 4.42.

Thiophenoxyketone 24. Thiocresol (945 mg, 7.61 mmol, 1.00 equiv) was added to 20 mL of pentane, followed by *N,N,N′,N′*-tetramethylethylenediamine (2.6 mL, 17 mmol, 2.3 equiv) via syringe. This mixture was stirred for 30 min and the flask was cooled in an IPA/dry ice bath. *n*-Butyllithium (10.3 mL, 15.4 mmol, 2.02 equiv) in hexane was added via gas-tight syringe over 15 min. The reaction mixture was stirred for 30 min then allowed to warm to ambient temperature, after which time the cloudy mixture was stirred for 17 h. The thick, white suspension was cooled in an ice bath and a solution of **23** (4.59 g, 15.2 mmol, 2.00 equiv) in 10 mL of pentane was added via cannula. After about 1 min the reaction mixture had become red and homogeneous. After 5 min, the solution was allowed to warm to ambient temperature and was stirred for 24 h. Toluene (50 mL) was added, followed by 100 mL 1 M HCl (aq), and both layers were transferred to a separatory funnel and separated. The aqueous layer was further acidified to pH 2 with conc. HCl and was added back to the organic layer and separated once more. The organic layer was washed with water (2 x 100 mL) then extracted with 5% aqueous NaOH (4 x 50 mL). The red NaOH extracts were combined, acidified (pH 1) with conc. HCl, and extracted with Et_2O (3 x 50 mL). The Et_2O extracts were combined and washed with water (2 x 100 mL) followed by

brine (100 mL) and dried over $MgSO_4$. The solvent was removed under vacuum, yielding a dark oil. The oil was dissolved in 100 mL CH_2Cl_2 and passed through a plug of silica. The solvent was once again removed under vacuum and the resulting yellow oil was diluted with 2 mL Et_2O. Pentane (5 mL) was added and the solution was cooled to -30 °C for 3 h. The yellow, microcrystalline product was collected by filtration and washed with cold pentane (5 x 1 mL) (2.70 g, 7.41 mmol, 97%). ^{1}H NMR (400 MHz, CD_2Cl_2): δ 8.21 (s, 2H), 8.13 (s, 1H), 7.38 (d, J = 8.0 Hz, 1H), 7.26 (m, 2H), 4.10 (s, 1H), 2.32 (s, 3H). ^{13}C{^{1}H} NMR (100.6 MHz, CD_2Cl_2): δ 194.15, 140.04, 135.81, 134.25, 133.80, 132.49, 132.23 (q, $J_{C\text{-}F}$ = 34.2 Hz), 131.89, 130.33, 130.30, 126.26 (quint, $J_{C\text{-}F}$ = 4.0 Hz), 123.41 (q, $J_{C\text{-}F}$ = 272.63 Hz), 20.79. ^{19}F NMR (376.5 MHz, CD_2Cl_2): δ -62.52. IR (cm^{-1}): 1663, 1652, 1611, 1559, 1471. Anal. Calcd. for $C_{16}H_{10}F_6OS$: C, 52.75; H, 2.77; S, 8.80. Found: C, 52.54; H, 2.93; S, 8.91.

L^{5}H (25). Molecular sieves (3 Å, 4.5 g), 15 mL of benzene, compound **24** (1.00 g, 2.74 mmol, 1.00 equiv) and *p*-toluidine (297 mg, 2.77 mmol, 1.01 equiv) were combined and left to stand for 10 d. The reaction mixture was then filtered away from the molecular sieves and lyophilized. The bright yellow residue was dissolved in 3 mL of Et_2O and 5 mL of pentane was slowly added while the solution was gently heated. The vessel was then cooled to -30 °C overnight. The crystalline solid was collected via filtration and washed with pentane (6 x 1 mL), yielding 878 mg of product. The pentane washes were added to the supernatant, which upon cooling afforded an additional 126 mg of pure **25** (1.00 g total, 2.21 mmol, 81%). ^{1}H NMR (400 MHz, C_6D_6): δ 8.43 (s, 2H), 7.79 (s, 1H), 6.90 (d, J = 8.0 Hz, 2H), 6.80 (d, J = 8.0 Hz, 2H), 6.75 (d, J = 8.0 Hz, 1H), 6.51 (m, 2H), 2.80 (s, 1H), 1.91 (s, 3H), 1.71 (s, 3H). ^{13}C{^{1}H} NMR (100.6 MHz, C_6D_6): δ 163.24, 147.56, 141.27, 136.35, 135.62, 134.70, 132.26 (q, $J_{C\text{-}F}$ = 33.2 Hz), 131.32, 130.74, 130.08, 129.54, 128.72 (d, $J_{C\text{-}F}$ = 3.0 Hz), 126.67, 124.04 (quint, $J_{C\text{-}F}$ = 4.0 Hz), 123.77 (q, $J_{C\text{-}F}$ = 273.6 Hz), 121.22, 20.75, 20.50. ^{19}F NMR (376.5 MHz, C_6D_6): δ -61.93. IR (cm^{-1}): 2563, 1627, 1596, 1504. Anal. Calcd. for $C_{23}H_{17}F_6NS$: C, 60.92; H, 3.78; N, 3.09; S, 7.07. Found: C, 61.04; H, 3.92; N, 2.90; S, 7.40.

$L^5Ni(PPh_3)Br$ (26). Ligand **25** (138 mg, 0.305 mmol, 1.00 equiv) was dissolved in 5 mL of THF and potassium *tert*-butoxide (35.0 mg, 0.312 mmol, 1.02 equiv) was added. The resulting homogeneous solution was stirred for 30 min. The L^5K solution was slowly added to a solution of $(Ph_3P)_2NiBr_2$ (227 mg, 0.305 mmol, 1.00 equiv) in 12 mL of THF. The reaction mixture rapidly became deep red/brown and cloudy in appearance. The solvent was then removed under vacuum after the reaction mixture was stirred for 3 h. The residue was extracted with 3 mL of CH_2Cl_2 and the extract was filtered. The resulting homogeneous solution was then gently heated while hexane (15 mL) was slowly added. Crystalline **26** formed upon cooling to -30 °C. The crystals were collected by filtration and washed with hexane (4 x 2 mL) (175 mg, 0.205 mmol, 67%). Note: ^{1}H NMR spectra of the crude reaction mixture show only the desired product and PPh_3; the purified yield reflects a difficulty in effecting complete removal of the liberated PPh_3. Crystals of suitable quality for X-ray diffraction analysis were grown by slow vapor diffusion of pentane into a benzene solution of **26**. ^{1}H NMR (500 MHz, C_6D_6): δ 7.91 (d, J = 7.5 Hz, 6H), 7.47 (d, J = 8.0 Hz, 2H), 7.41 (s, 2H), 7.34 (d, J = 8.0 Hz, 1H), 7.29 (s, 1H), 7.06 (m, 6H), 6.91 (m, 5H), 6.73 (d, J = 7.5 Hz, 1H), 6.65 (s, 1H), 2.14 (s, 3H), 1.96 (s, 3H). ^{13}C{^{1}H} NMR (125.8 MHz, CD_2Cl_2): δ 164.28, 147.73, 146.69, 145.97, 139.96, 137.47, 137.17, 134.79, 133.13, 131.66 (q, J_{C-F} = 34.0 Hz), 131.37, 130.33, 129.91, 128.44, 127.77, 126.56, 123.49, 123.30 (q, J_{C-F} = 273.0 Hz), 20.26, 20.17. ^{19}F NMR (376.5 MHz, CD_2Cl_2): δ -62.62. IR (cm^{-1}): 1532, 1495, 1480, 1431. Anal. Calcd. for $C_{41}H_{31}BrF_6NNiPS \cdot 1.5C_6H_6$: C, 61.88; H, 4.15; N, 1.44. Found: C, 61.68; H, 3.99; N, 1.40.

$L^5Pt(PPh_3)_2Cl$ (27). Ligand **25** (71.0 mg, 0.157 mmol, 1.00 equiv) was dissolved in 5 mL of THF and potassium *tert*-butoxide (18.0 mg, 0.160 mmol, 1.02 equiv) was added. The resulting homogeneous solution was stirred for 30 min. The L^5K solution was slowly added to a suspension of $(Ph_3P)_2PtCl_2$ (124 mg, 0.156 mmol, 0.993 equiv) in 10 mL of THF. The reaction mixture was stirred overnight. The solvent was then removed under vacuum, and the residue was dissolved in 8 mL of benzene, filtered and lyophilized. ^{1}H NMR spectra of the crude material indicated near quantitative conversion to the desired product. The crude solid was dissolved in 1.5 mL CH_2Cl_2, into which Et_2O vapor was allowed to slowly diffuse. This procedure afforded crystalline material suitable for X-ray structural analysis (107 mg,

0.0886 mmol, 56%). ^{1}H NMR (400 MHz, CD_2Cl_2): δ 8.07 (s, 2H), 7.86 (s, 1H), 7.68 (d, J = 8.4 Hz, 1H), 7.42-7.25 (m, 18H), 7.18-7.09 (m, 12H), 6.93 (d, J = 8.0 Hz, 1H), 6.84 (d, J = 8.0 Hz, 2H), 6.79 (d, J = 8.0 Hz, 2H), 6.43 (s, 1H), 2.19 (s, 3H), 2.10 (s, 3H). ^{13}C{^{1}H} NMR (125.8 MHz, CD_2Cl_2): δ 166.48, 148.47, 142.62, 139.55, 138.29, 137.01, 135.57, 135.49, 134.78, 134.70, 133.69, 133.57, 131.25, 130.88 (q, $J_{C\text{-}F}$ = 25.2 Hz), 130.84, 129.34, 128.35, 128.33, 128.26, 128.25, 124.22 (q, $J_{C\text{-}F}$ = 271.7 Hz), 123.14, 121.85, 21.14, 21.11. ^{31}P{^{1}H} NMR (162.0 MHz, CD_2Cl_2): δ 19.02 (d with Pt sat., $J_{P\text{-}P}$ = 19.4 Hz, $J_{P\text{-}Pt}$ = 2796 Hz), 18.16 (d with Pt sat., $J_{P\text{-}P}$ = 19.4 Hz, $J_{P\text{-}Pt}$ = 3865 Hz). ^{19}F NMR (376.5 MHz, CD_2Cl_2): δ -61.92. IR (cm^{-1}): 1622, 1592, 1500, 1478. Anal. Calcd. for $C_{59}H_{46}ClF_6NP_2PtS$: C, 58.68; H, 3.84; N, 1.16. Found: C, 58.61; H, 4.04; N, 1.23.

[L^{5}Rh(cod)]$_2$ (28). Potassium *tert*-butoxide (13.8 mg, 0.123 mmol, 1.00 equiv) was added to a solution of **25** (55.6 mg, 0.123 mmol, 1.00 equiv) in 3 mL of THF. After stirring for 30 min, the mixture was added dropwise to a solution of $[Rh(cod)Cl]_2$ (30.2 mg, 0.0612 mmol, 0.498 equiv) in 10 mL of THF. The reaction mixture was stirred for 3 h, after which time the solvent was removed under reduced pressure. The residue was extracted with 2 mL of benzene and the extract was filtered into a small vessel, into which 1 mL of pentane vapor was allowed to slowly diffuse. Large crystals of [**28**·0.5 pentane] were collected and washed with Et_2O (3 x 1 mL) (56.8 mg, 0.0813 mmol, 66%). ^{1}H NMR spectra of **28** at three temperatures are included in the Supporting Information. These spectra, as well as the elemental analysis, were obtained using the same sample that was used for the X-ray diffraction studies. IR (cm^{-1}): 1630, 1604, 1595, 1504. Anal. Calcd. for $C_{31}H_{28}F_6NRhS·0.5C_5H_{12}$: C, 57.51; H, 4.90; N, 2.00. Found: C, 57.39; H, 5.03; N, 2.00.

Acknowledgements

We are indebted to Dr. Fred Hollander and Dr. Allen Oliver at the UC Berkeley CHEXRAY X-ray crystallographic facility and Dr. Kathleen Durkin at the Molecular Graphics Facility (NSF grant CHE-0233882) for crystallographic and computational consultation, respectively. We also thank Prof. F. Dean Toste for advice concerning ligand syntheses. This work was supported by NSF grant CHE-0345488 to R.G.B. and DOE funding to J.A.

Supporting Information Available: CIF-format files for all crystallographically determined structures, NMR spectra of **16**, **19**, **20** and **28**, positional coordinates of all computed structures. This material is available free of charge via the Internet at http:/pubs.acs.org.

References

(1) Jacobsen, E. N.; Zhang, W.; Muci, A. R.; Ecker, J. R.; Deng, L. *J. Am. Chem. Soc.* **1991**, *113*, 7063-7064.

(2) a) Matsui, S.; Mitani, M.; Saito, J.; Tohi, Y.; Makio, H.; Matsukawa, N.; Takagi, Y.; Tsuru, K.; Nitabaru, M.; Nakano, T.; Tanaka, H.; Kashiwa, N.; Fujita, T. *J. Am. Chem. Soc.* **2001**, *123*, 6847-6856; b) Mitani, M.; Furuyama, R.; Mohri, J.; Saito, J.; Ishii, S.; Terao, H.; Kashiwa, N.; Fujita, T. *J. Am. Chem. Soc.* **2002**, *124*, 7888-7889; c) Hustad, P. D.; Coates, G. W. *J. Am. Chem. Soc.* **2002**, *124*, 11578-11579.

(3) a) Wang, C. M.; Friedrich, S.; Younkin, T. R.; Li, R. T.; Grubbs, R. H.; Bansleben, D. A.; Day, M. W. *Organometallics* **1998**, *17*, 3149-3151; b) Younkin, T. R.; Conner, E. F.; Henderson, J. I.; Friedrich, S. K.; Grubbs, R. H.; Bansleben, D. A. *Science* **2000**, *287*, 460-462.

(4) Connor, E. F.; Younkin, T. R.; Henderson, J. I.; Waltman, A. W.; Grubbs, R. H. *Chem. Commun.* **2003**, 2272-2273.

(5) a) Kerber, W. D.; Nelsen, D. L.; White, P. S.; Gagne, M. R. *Dalton* **2005**, 1948-1951; b) Alteparmakian, V.; Robinson, S. D. *Inorg. Chim. Acta* **1986**, *116*, L37-L38; c) Leipoldt, J. G.; Basson, S. S.; Grobler, E. C.; Roodt, A. *Inorg. Chim. Acta* **1985**, *99*, 13-17; d) Bonnaire, R.; Potvin, C.; Manoli, J. M. *Inorg. Chim. Acta* **1980**, *45*, L255-L256.

(6) a) Chatterjee, D.; Mitra, A.; Roy, B. C. *React. Kinet. Catal. Lett.* **2000**, *70*, 147-151; b) Anderson, D. J.; Eisenberg, R. *Organometallics* **1996**, *15*, 1697-1706; c) El-Hendawy, A. M.; Alkubaisi, A. H.; El-Kourashy, A. E.; Shanab, M. M. *Polyhedron* **1993**, *12*, 2343-2350; d) Pasini, A.; Caldirola, C.; Colombo, A.; Ghilotti, M. *J. Organomet. Chem.* **1988**, *345*, 201-208.

(7) a) Sariego, R.; Carkovic, I.; Martinez, M. *Transition Met. Chem.* **1984**, *9*, 106-108; b) Mague, J. T.; Nutt, M. O. *J. Organomet. Chem.* **1979**, *166*, 63-77.

(8) a) Marin-Becerra, A.; Stenson, P. A.; McMaster, J.; Blake, A. J.; Wilson, C.; Schroder, M. *Eur. J. Inorg. Chem.* **2003**, 2389-2392; b) Kaasjager, V. E.; Puglisi, L.; Bouwman, E.; Driessen, W. L.; Reedijk, J. *Inorg. Chim. Acta* **2000**, *310*, 183-190; c) Mugesh, G.; Singh, H. B.; Butcher, R. J. *Eur. J. Inorg. Chem.* **1999**, 1229-1236; d) Goswami, N.; Eichhorn, D. M. *Inorg. Chem.* **1999**, *38*, 4329-4333; e) Marini, P. J.; Berry, K. J.; Murray, K. S.; West, B. O.; Irving, M.; Clark, P. E. *J. Chem. Soc., Dalton Trans.* **1983**, 879-884.

(9) a) Hoskins, B. F.; Robson, R.; Williams, G. A.; Wilson, J. C. *Inorg. Chem.* **1991**, *30*, 4160-4166; b) Hoskins, B. F.; McKenzie, C. J.; Robson, R.; Lu, Z. R. *J. Chem. Soc., Dalton Trans.* **1990**, 2637-2641.

(10) a) Fallon, G. D.; Nichols, P. J.; West, B. O. *J. Chem. Soc., Dalton Trans.* **1986**, 2271-2276; b) Marini, P. J.; Murray, K. S.; West, B. O. *J. Chem. Soc., Dalton Trans.* **1983**, 143-151; c) Marini, P. J.; Murray, K. S.; West, B. O. *J. Chem. Soc., Chem. Commun.* **1981**, 726-728.

(11) Akine, S.; Nabeshima, T. *Inorg. Chem.* **2005**, *44*, 1205-1207.

(12) Corrigan, M. F.; Rae, I. D.; West, B. O. *Aust. J. Chem.* **1978**, *31*, 587-594.

(13) a) Frydendahl, H.; Toftlund, H.; Becher, J.; Dutton, J. C.; Murray, K. S.; Taylor, L. F.; Anderson, O. P.; Tiekink, E. R. T. *Inorg. Chem.* **1995**, *34*, 4467-4476; b) Other methods available, see Garnovskii, A. D.; Nivorozhkin, A. L.; Minkin, V. I. *Coord. Chem. Rev.* **1993**, *126*, 1-69.

(14) Olekhnovich, L. P.; Kurbatov, V. P.; Osipov, O. A.; Minkina, L. S.; Minkin, V. I. *J. Gen. Chem. USSR* **1968**, *38*, 2512.

(15) Iron complex of L^2 has previously been prepared, see ref. 10b.

(16) $Ir(cod)_2Cl$ used as iridium source in reported synthetic procedure, giving identical results.

(17) Due to the number of structures present in this report, comments will be made only on structural features pertinent to this study. CIF-format files for all structures can be found in the Supporting Information.

(18) Duff, S. E.; Barclay, J. E.; Davies, S. C.; Hitchcock, P. B.; Evans, D. J. *Eur. J. Inorg. Chem.* **2005**, 4527-4532.

(19) a) Nikiforov, G. B.; Roesky, H. W.; Magull, J.; Labahn, T.; Vidovic, D.; Noltemeyer, M.; Schmidt, H. G.; Hosmane, N. S. *Polyhedron* **2003**, *22*, 2669-2681; b) Basuli, F.; Bailey, B. C.; Tomaszewski, J.; Huffman, J. C.; Mindiola, D. J. *J. Am. Chem. Soc.* **2003**, *125*, 6052-6053.

(20) a) Karsten, P.; Strahle, J. *Acta Crystallogr., Sect. C: Cryst. Struct. Commun.* **1999**, *C55*, 488-489; b) Coombes, R. C.; Costes, J. P.; Fenton, D. E. *Inorg. Chim. Acta* **1983**, *77*, L173-L174.

(21) Corrigan, M. F.; West, B. O. *Aust. J. Chem.* **1976**, *29*, 1413-1427.

(22) a) Mann, G.; Baranano, D.; Hartwig, J. F.; Rheingold, A. L.; Guzei, I. A. *J. Am. Chem. Soc.* **1998**, *120*, 9205-9219; b) Osakada, K.; Maeda, M.; Nakamura, Y.; Yamamoto, T.; Yamamoto, A. *J. Chem. Soc., Chem. Commun.* **1986**, 442-443.

(23) Hall, J. R.; Swile, G. A. *Aust. J. Chem.* **1975**, *28*, 1507-1511.

(24) Budzelaar, P. H. M.; van Oort, A. B.; Orpen, A. G. *Eur. J. Inorg. Chem.* **1998**, 1485-1494.

(25) a) Bouwman, E.; Henderson, R. K.; Powell, A. K.; Reedijk, J.; Smeets, W. J. J.; Spek, A. L.; Veldman, N.; Wocadlo, S. *J. Chem. Soc., Dalton Trans.* **1998**, 3495-3499; b) Christensen, A.; Jensen, H. S.; McKee, V.; McKenzie, C. J.; Munch, M. *Inorg. Chem.* **1997**, *36*, 6080-6085.

(26) Guner, V.; Khuong, K. S.; Leach, A. G.; Lee, P. S.; Bartberger, M. D.; Houk, K. N. *J. Phys. Chem. A* **2003**, *107*, 11445-11459.

(27) Alaimo, P. J.; Peters, D. W.; Arnold, J.; Bergman, R. G. *J. Chem. Ed.* **2001**, *78*, 64.

(28) Still, I. W. J.; Natividad-Preyra, R.; Toste, F. D. *Can. J. Chem.* **1999**, *77*, 113-121.

(29) Kagano, H.; Itsuda, H.; Yoshida, K.; Nakano, M. (Sumitomo Seika KK, Japan). Jpn. Kokai Tokkyo Koho 05246981, 1993.

(30) Adams, R.; Reifschneider, W.; Ferretti, A. *Organic Syntheses* **1962**, *42*, 22-25.

(31) Herde, J. L.; Lambert, J. C.; Senoff, C. V. *Inorganic Syntheses* **1974**, *15*, 18-20.

(32) Giordano, G.; Crabtree, R. H. *Inorganic Syntheses* **1979**, *19*, 218-220.

(33) Appleton, T. G.; Hall, J. R.; Williams, M. A. *J. Organomet. Chem.* **1986**, *303*, 139-149.

(34) Chatt, J.; Shaw, B. L. *J. Chem. Soc.* **1959**, 705-716.

(35) Roulet, R.; Barbey, C. *Helv. Chim. Acta* **1973**, *56*, 2179-2186.

(36) a) Adapted from Puddephatt, R. J.; Thompson, P. J. *J. Chem. Soc., Dalton Trans.* **1977**, 1219-1223; b) Spectra match Davies, J. A.; Eagle, C. T.; Otis, D. E.; Venkataraman, U. *Organometallics* **1989**, *8*, 1080-1088.

(37) Hidai, M.; Kashiwag.T; Ikeuchi, T.; Uchida, Y. *J. Organomet. Chem.* **1971**, *30*, 279-&.

(38) Onderdelinden, A. L.; Van der Ent, A. *Inorg. Chim. Acta* **1972**, *6*, 420-426.

(39) *SMART: Area-Detector Software Package;* Bruker AXS: Madison, WI, 2001-2003.

(40) *SAINT: SAX Area Detector Integration Program*, version 6.40; Bruker AXS: Madison, WI, 2003.

(41) *XPREP*, version 6.12; part of the SHELXTL Crystal Structure Determination Package; Bruker AXS: Madison, WI, 2001.

(42) *SADABS: Bruker-Nonius Area Detector scaling and Absoption Correction Program*, version 2.05; Bruker AXS: Madison, WI, 2003.

(43) *teXsan: Crystal Structure Analysis Package;* Molecular Structure Corporation, 1985 & 1992.

(44) Farrugia, L. J. *J. Appl. Cryst.* **1997**, *30*, 565.

(45) *Jaguar,* version 5.5; Schrodinger, LLC: Portland, OR, 2003.

(46) *Maestro*, version 6.5; Schrodinger, LLC: Portland, OR, 2004.

(47) Stephens, P. J.; Devlin, F. J.; Chabalowski, C. F.; Frisch, M. J. *J. Phys. Chem.* **1994**, *98*, 11623-11627.

(48) Becke, A. D. *J. Chem. Phys.* **1993**, *98*, 5648-5652.

(49) Miehlich, B.; Savin, A.; Stoll, H.; Preuss, H. *Chem. Phys. Lett.* **1989**, *157*, 200-206.

(50) Hay, P. J.; Wadt, W. R. *J. Chem. Phys.* **1985**, *82*, 299-310.

(51) a) Francl, M. M.; Pietro, W. J.; Hehre, W. J.; Binkley, J. S.; Gordon, M. S.; DeFrees, D. J.; Pople, J. A. *J. Chem. Phys.* **1982**, *77*, 3654-3665; b) Hariharan, P. C.; Pople, J. A. *Theor. Chim. Acta* **1973**, *28*, 213-222; c) Hehre, W. J.; Ditchfield, R.; Pople, J. A. *J. Chem. Phys.* **1972**, *56*, 2257-2261; d) Ditchfield, R.; Hehre, W. J.; Pople, J. A. *J. Chem. Phys.* **1971**, *54*, 724-728.

(52) a) Frisch, M. J.; Pople, J. A.; Binkley, J. S. *J. Chem. Phys.* **1984**, *80*, 3265-3269; b) Clark, T.; Chandrasekhar, J.; Spitznagel, G. W.; Schleyer, P. V. *J. Comput. Chem.* **1983**, *4*, 294-301; c) McLean, A. D.; Chandler, G. S. *J. Chem. Phys.* **1980**, *72*, 5639-5648; d) Krishnan, R.; Binkley, J. S.; Seeger, R.; Pople, J. A. *J. Chem. Phys.* **1980**, *72*, 650-654.

(53) Topolski, M. *J. Org. Chem.* **1995**, *60*, 5588-5594.

For table of contents use only:

Title: Platinum Group Thiophenoxyimine Complexes: Syntheses, Crystallographic and Computational Studies of Structural Properties.

Authors: Jamin L. Krinsky, John Arnold,* Robert G. Bergman*

Abstract: Syntheses and ligand-substitution chemistry of monomeric thiophenoxyimine complexes of rhodium, iridium, nickel and platinum are reported. Crystallographic and computational investigation showed that the size of the substituent on the imine carbon has a large effect on ligand conformation and coordination behavior.